UNIVERSITY OF CALIFORNIA
RIVERSIDE

Effects of Surface Treatments in Metal-on-Oxide Surfaces Studied by Low Energy Ion Scattering

A Dissertation submitted in partial satisfaction
of the requirements for the degree of

Doctor of Philosophy

in

Physics

by

Alex B. Arjad

March 2014

Dissertation Committee:

Dr. Jory A. Yarmoff, Chairperson
Dr. Ward Beyermann
Dr. Allen Mills

The Dissertation of Alex B. Arjad is approved:

_____

_____

_____
Committee Chairperson

University of California, Riverside

Acknowledgments

This work would not have been possible without a number of people. First and most obviously is my adviser, Dr. Jory Yarmoff. As a scientist, his depth of knowledge of the science, the scientific literature, and of experimental technique is impressive. As a manager, he is readily available to students with advice or assistance but also knows when a student is best left to their work. I am fortunate for having Dr. Yarmoff alone, but I am also fortunate on account of the co-workers I have spent many of these years with. For most of my graduate career I enjoyed the company of now Dr. Reuben Gann, who helped me with many of the finer points of equipment repair and construction during my time here, as well as assistance with programming, and many other useful discussions besides. I also had excellent co-workers in Dr. Snejana "Snow" Balaz and Dr. Xiaoxiao He.

I would also like to thank my mother and father, Henry and Laura Arjad, for their unwavering support during my entire education, and for never doubting me for a moment, even as I doubted myself. My brother Alen Arjad and my cousin Adeline Arjad also have been generous in their encouragement.

This work was also supported by the NSF under CHE-1012987

Chapter 2 was reprinted with permission from Journal of Physical Chemistry C, A. B. Arjad and J. A. Yarmoff, Ion-Impact-Induced Strong Metal Surface Interaction in $Pt/TiO_2(110)$, **2012**, *116* (44), pp 23377–23382 Copyright 2012, American Chemical Society

Chapter 3 was reprinted from Nuclear Instruments and Methods in Physics Research Section B: Beam Interactions with Materials and Atoms, Vol 317, A. B. Arjad and J. A. Yarmoff, Temperature dependence of the neutralization of low energy K^+ ions scattered from Au nanoclusters on SiO_2, pp 13-17, **2013**, with permission from Elsevier

ABSTRACT OF THE DISSERTATION

Effects of Surface Treatments in Metal-on-Oxide Surfaces Studied by Low Energy Ion Scattering

by

Alex B. Arjad

Doctor of Philosophy, Graduate Program in Physics
University of California, Riverside, March 2014
Dr. Jory A. Yarmoff, Chairperson

Low energy ion scattering (LEIS) is a technique found to be sensitive to the structural and electronic properties of metal on oxide systems. Here, LEIS is used to investigate the effect of sputtering Pt deposited on TiO_2 as well as the effect of surface temperature on Au nanoclusters on SiO_2. In the case of Pt/TiO_2, it was found that sputtering induces a "strong metal-surface interaction" (SMSI) state, where the surface atoms become mobilized and move to cover the Pt. Previously, this state has been observed when heating the sample, but in this case the sputter beam was found to mobilize the substrate atoms instead of an elevated temperature. K^+ scattering was used to examine Au/SiO_2 at temperatures ranging from 100 to 300 K. It was found that the probability that an ion would be neutralized during scattering is inversely and reversibly proportional to the temperature. Finally, Na^+ was used to examine Au/SiO_2 after annealing to temperatures ranging from 300 to 1000 K. It was found that the neutralization probability is dependent not only upon the annealing temperature, but also whether the ion undergoes single or multiple scattering. The ratio of single scattering to multiple scattering neutralization probability may provide another tool to analyze surface evolution.

Contents

Chapter 4

List of figures

List of tables

Chapter 1

Introduction

1.1 Metal nanoclusters

Understanding the properties of supported nanoclusters is a very important problem in nanoscience and surface science. These properties of such nanostructures are very different from the bulk material, to the point that it can seem like rediscovering the periodic table of the elements. One striking example is the structural and catalytic properties of nano-scale gold. The bulk metal forms a close-packed cubic structure, while on the nano-scale, gold can form 2D structures, hemispheres [1] , or even fractals [2], depending on the growth conditions. The catalytic properties, however, are even more interesting. Haruta discovered that supported gold nanoclusters are catalytically active for a number of reactions [3]. One of these is CO oxidation, of particular interest for ecological and industrial applications. Gold nanoclusters on TiO_2 have been found to be catalytically active for CO oxidation even at temperatures of -70˚C, while bulk gold is only active 400 K and higher [4]. The properties of gold nanoclusters are also size dependent. For instance, the turnover frequency of CO oxidation for gold nanoclusters on TiO_2 is at a maximum for 3 nm diameter clusters. This is not to say that interest in supported metal nanoclusters is limited to Au/TiO_2, however. Many supported metal nanoclusters systems have been shown to be active nanocatalysts, such as Pt/TiO_2 [5], Au/SiO_2 [6], $Ag/BaTiO_3$ [7], and Al/HOPG [8].

1.1.1 Evolution of the surface

The work in this thesis is primarily concerned with metal nanoclusters initially deposited by evaporating metal nanoclusters from a hot filament, a method that is called Physical Vapor Deposition (PVD). Subsequent treatments are then used to modify the clusters. For instance, metal nanoclusters may change size and shape when exposed to sputter beams, high pressure, or temperature changes. Because the electronic, chemical, and physical properties of the clusters change with size and shape, the nanocluster-dependent device can be compromised or even destroyed during what might be normal use for a conventional device of that class. For instance, a nanocluster dependent catalyst might be exposed to high temperature, causing the clusters to sinter, with small clusters merging to become larger clusters. In addition to cluster sintering, additional modes of surface evolution are described below.

1.1.2 Ostwald ripening

One type of surface evolution is called Ostwald ripening. During Ostwald ripening, large particles grow at the expense of smaller ones. This happens because larger particles are more thermodynamically stable, as they have proportionally fewer surface atoms. Surface atoms can break off of a cluster and seek a more thermodynamically favorable configuration, probably by attaching to larger cluster. This creates a bimodal distribution of cluster sizes [9] as the "donor" clusters become smaller while the "acceptor" cluster increase in size. Eventually, the smaller clusters will be consumed. Increasing the surface temperature accelerates this effect.

1.1.3 Strong metal surface interaction

Another type of well-known surface evolution is the Strong Metal-Surface Interaction (SMSI). It was observed that the catalytic activity of Pt/TiO_2 was suppressed after annealing to 500˚C [10]. To explain this, it was proposed that the substrate atoms might encapsulate the metal. This happens because the thermal energy mobilizes the substrate atoms, and there is a more thermodynamically favorable state where the oxide is on top of the metal. Evidence accumulated for the hypothesis [11] and finally atomic resolution STM images and ion scattering experiments confirmed it [5].

1.2 Ion scattering

One of the standard techniques used to probe supported nanoclusters is ion scattering. Scattering itself is a phenomenon of fundamental importance, explaining such diverse phenomena as the collisions of macroscopic objects, the color of the sky, and image contrast in Transmission Electron Microscopy. Because of this importance, scattering has attracted a great deal of theoretical and experimental interest from great figures like Isaac Newton and James Clerk Maxwell. Max Born has also written a great deal about scattering from a quantum mechanical perspective.

Quantum mechanics aside, the classical theory of scattering is sophisticated and well developed. The problem can be solved for two particles if the potential is known and depends only upon the separation of the particles. Given the impact parameter, or the closest approach in the absence of scattering, the final trajectory of the particles can be calculated.

This does not always suffice, however. Many body interactions greatly complicate calculations, and potentials must be determined semi-empirically by fitting parameters to experimental data. Fortunately, through appropriate experimental design, we can operate in a regime that greatly simplifies the problem and sidesteps these complications.

1.2.1 Ion scattering as a surface science tool

The work in this thesis concerns itself primarily with Low Energy Ion Scattering (LEIS), which is the scattering of charged atomic particles in the 500 eV to 5 keV range. The scattering problem is greatly simplified in this regime because the collisions are binary in nature, which means that the ion only interacts with one atom at a time. As a consequence, the energy of the singly scattered ions can be easily calculated using simple conservation of energy and momentum considerations instead of using a more sophisticated scattering formalism, which would require detailed knowledge of the scattering potential. Ion scattering is also highly surface sensitive in this regime, penetrating at most a few atomic layers. Finally, the projectiles chosen for this experiment are alkali ions, for which the primary neutralization mechanism is Resonant Charge Transfer (RCT). RCT is particularly sensitive to electronic states near the Fermi energy. This sensitivity means that the neutralization probability of scattered ions can reveal information about the clusters' Local Electrostatic Potential (LEP).

Low energy ion scattering employing alkali ions has a number of desirable properties that cannot be found together in other techniques. In particular, it is highly surface sensitive, sensitive to local electronic conditions, and sensitive to electronic states

near the Fermi level. In contrast, photon and electron spectroscopies tend to be sensitive to a few tens of layers. Although UPS is sensitive to states near the Fermi level, photoelectrons come from the substrate as well as the nanoclusters, complicating analysis. He^+ ion scattering, while it is even more surface sensitive than alkali ion LEIS and a common technique, is also inadequate because its neutralization is driven primarily by Auger neutralization so that electronic information about the nanoclusters cannot be obtained.

1.2.2 Energy of singly scattered particles

In principle, calculating the energies of ions scattered from a surface requires a quantum mechanical treatment of the many interacting bodies near the scattering site and the scattering bodies themselves. In practice, a number of simplifications can be made with little loss of predictive power. In the LEIS regime, the scattering cross sections are smaller than the inter-atomic spacing enabling the use of the Binary Collision Approximation (BCA), in which the projectiles are treated as though they interact with a single atom at a time during the entire scattering process. Furthermore, the de Broglie wavelength of the scattered ions is on order of 10^{-13} m, so that diffraction effects can also be ignored. Thus, the energy of the singly scattered particles can be calculated by using elementary classical mechanics.

In this derivation, we will use the subscripts "1" to denote the projectile, "2" to denote the target, "i" to denote conditions before scattering, and "f" to denote conditions after scattering. For instance, "v_{1f}" denotes the velocity of the projectile after scattering.

Let us start with momentum considerations. The target atom is nearly stationary, so this yields…

$$m_1\vec{v}_{1i} = m_1\vec{v}_{1f} + m_2\vec{v}_{2f} \quad (1)$$

Rearrange…

$$m_1\left(\vec{v}_{1i} - \vec{v}_{1f}\right) = m_2\,\vec{v}_{2f}$$

Square both sides…

$$m_1^2\left(v_{1i}^2 + v_{1f}^2 - 2\vec{v}_{1i}\cdot\vec{v}_{1f}\right) = m_2^2v_{2f}^2$$

To simplify, let us also define a reduced mass μ such that $\mu=m_2/m_1$, as well as the angle θ between the projectile's initial and final trajectory.

$$v_{1i}^2 + v_{1f}^2 - 2v_{1i}v_{1f}\cos\theta = \mu^2v_{2f}^2 \quad (2)$$

We now turn to conservation of energy.

$$\tfrac{1}{2}m_1v_{1i}^2 = \tfrac{1}{2}m_1v_{1f}^2 + \tfrac{1}{2}m_2v_{2f}^2 \quad (3)$$

Cancel factors of 0.5 and group terms in m_1…

$$m_1(v_{1i}^2 - v_{1f}^2) = m_2v_{2f}^2$$

Dividing both sides by m_1 and substituting the reduced mass yields…

$$v_{1i}^2 - v_{1f}^2 = \mu v_{2f}^2 \quad (4)$$

Now we can multiply both sides of (4) by μ, then substitute into the RHS of (2) so as to eliminate v_{2f}…

$$v_{1i}^2 + v_{1f}^2 - 2v_{1i}v_{1f}\cos\theta = \mu(v_{1i}^2 - v_{1f}^2)$$

Now move everything to the LHS and gather terms in v_{1f}…

$$(1+\mu)\,v_{1f}^2 - 2v_{1i}v_{1f}\cos\theta + (1-\mu)v_{1i}^2 = 0$$

This is now recognizable as a quadratic equation in v_{1f}. A survey of the rest of the variables confirms that they are set by the experimental design, and thus known. Applying the quadratic formula yields

$$v_{1f} = \frac{2v_{1i}\cos\theta \pm \sqrt{(2v_{1i}\cos\theta)^2 - 4(1+\mu)(1-\mu)v_{1i}^2}}{2(1+\mu)} \quad (4)$$

Evaluating the parenthesis yields…

$$v_{1f} = \frac{2v_{1i}\cos\theta \pm \sqrt{(4v_{1i}^2\cos^2\theta) - 4(1-\mu^2)v_{1i}^2}}{2(1+\mu)}$$

Now cancel a factor of 2 from both numerator and denominator, and factor out v_{1i} from the numerator…

$$v_{1f} = v_{1i}\,\frac{\cos\theta \pm \sqrt{\cos^2\theta - (1-\mu^2)}}{(1+\mu)}$$

Now simplify the discriminant and apply the Pythagorean trig identity…

$$v_{1f} = v_{1i}\,\frac{\cos\theta \pm \sqrt{\mu^2 - \sin^2\theta}}{(1+\mu)} \quad (5)$$

In order for this to be physically allowed, the discriminant must be positive…

$$\frac{m_2}{m_1} \geq \sin^2\theta$$

…which is only true in general if the mass of the target is greater than or equal to the mass of the projectile. For this reason, we use light projectiles scattering from heavy targets, so that backscattering ($\theta > 90^\circ$) is always possible.

From (5), it is trivial to find the energy of the scattered particles.

$$E_{1f} = \frac{1}{2} m_1 v_{1f}^2 = \frac{1}{2} m_1 v_{1i}^2 \left[\frac{\cos\theta \pm \sqrt{\mu^2 - \sin^2\theta}}{(1+\mu)} \right]^2 = E_{1i} \left[\frac{\cos\theta \pm \sqrt{\mu^2 - \sin^2\theta}}{(1+\mu)} \right]^2 \quad (6)$$

Thus, knowing the initial and final energy of the singly scattered ion, as well as the mass of the scattered ion, we can determine the mass, and hence the identity, of the target atom.

1.2.3 Multiple and plural scattering

In addition to single scattering, there are two other types of scattering that can occur during LEIS. One is plural scattering (PS), during which the ion scatters two or more times in-plane before arriving at the detector. Particles that undergo plural scattering will arrive at the detector with higher energy than singly scattered particles. This is the case because a particle scattering once through 150° loses more energy than the same particle scattering twice through angles that result in a total scattering angle of 150°. An example of this process is illustrated below.

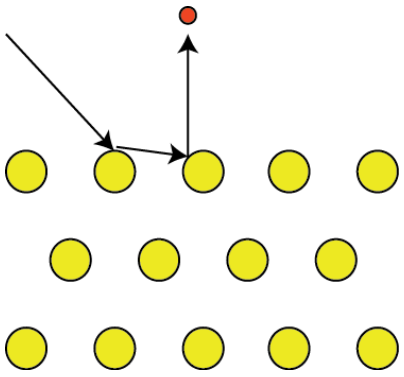

Figure 1.1 Illustration of a plural scattering trajectory

Multiple scattering (MS), on the other hand, occurs when a particle experiences multiple out of plane collisions before reaching the detector. In this case, inelastic losses will

result in the particle having less energy than the singly scattered ions. An example of this process is illustrated below.

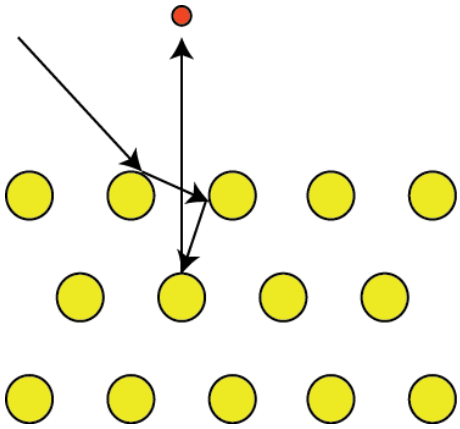

Figure 1.2 Illustration of a multiple scattering trajectory

Single, multiple, and plural scattering are all visible in an ion scattering spectrum. A spectrum of 2 keV Na^+ ions scattering from 2 Å of Au deposited on SiO_2 is shown below, with the single scattering peak (SSP), plural scattering, and multiple scattering regions labeled. The area below the smooth curve corresponds to a background of recoiled surface atoms.

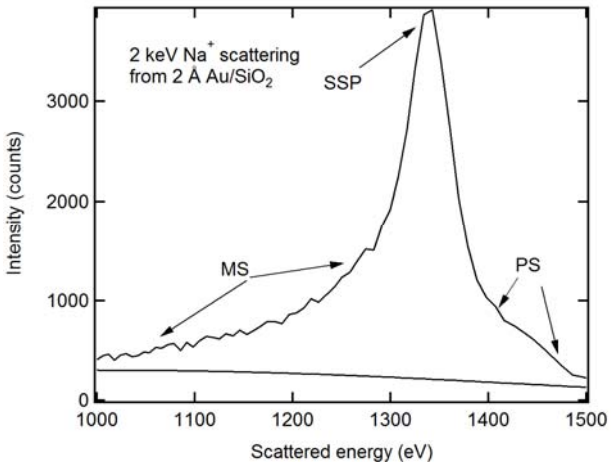

Figure 1.3 A typical ion scattering spectrum.

1.3. Resonant Charge Transfer

Neutralization during LEIS with alkali ions is primarily driven by Resonant Charge Transfer (RCT), where electrons are exchanged between two states close to each other in energy. The RCT process is diagrammed in the figure below.

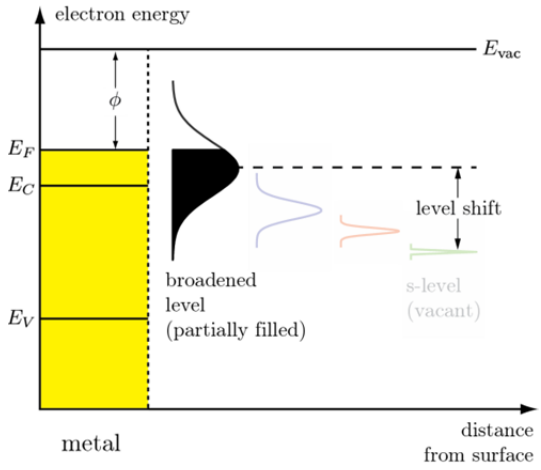

Figure 1.4 Schematic of the energy shifting as the ion approaches the surface.

During RCT, the energy level shifts and broadens as described in detail below. In scattering from a flat surface, the final charge state would be a function of the perpendicular component of the exit velocity. For instance, an extremely fast ion would leave the surface before any charge could be exchanged, resulting in a neutralization probability fraction of 0. In the opposite, adiabatic case, an extremely slow ion would have a neutral fraction of either 0 or 1, determined by the relative values of the work function and the ionization energy. During LEIS, however, the ion moves quickly enough so as to be non-adiabatic but not so quickly that no charge can be exchanged. This gives rise to an effective "freezing distance," or an apparent distance above the surface at which the charge state is determined. Because the ionization level still has

some width at this distance, it can be partially neutralized. This is measured as a neutralization probability.

1.3.1 Level shifting

The shifting of the ionization level can be determined from electrostatic considerations. The electric potential of a collection of charges near a metal surface can be determined using the method of images, as diagrammed below.

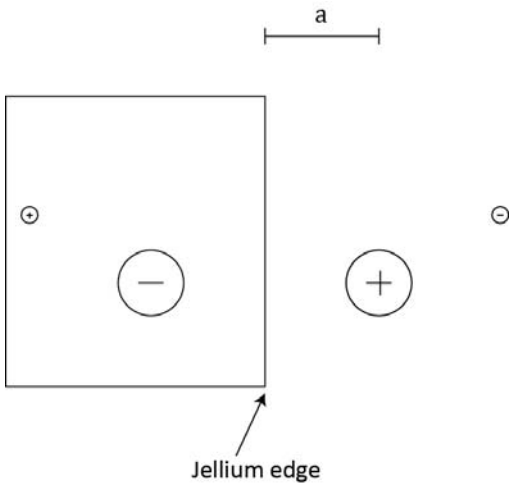

Figure 1.5 The shifted ionization level must be calculated with the image charges in mind.

Let us consider an ion core a small distance "*a*" from a metal surface, as it would be during scattering. Recall that the energy level of a bound electron is the potential energy difference between the electron at infinity and the electron being in the bound state. In order to calculate the energy shift from the normal ionization level, we consider the work necessary to move an electron from infinity to its bound state in this configuration as compared to a configuration without the metal. As seen in the above diagram, there are two differences between the configuration near a metal surface and the

configuration without the metal. The first is the image of the ion core, which is stationary as the electron is brought in from infinity. The second is the image of the electron, which starts at –infinity and moves closer to the surface as the electron does. We can now calculate the work that the electron does against its image as it moves toward the ion core due to the Coulomb force…

$$W = \int \vec{F} \cdot d\vec{r}$$

$$W = \int_{\infty}^{a} \frac{q^2}{4\pi\epsilon_0}\left(\frac{1}{2z}\right)^2 dz$$

$$W = \frac{q^2}{16\pi\epsilon_0}\int_{\infty}^{a}\left(\frac{1}{z}\right)^2 dz$$

$$W = -\frac{q^2}{16\pi\epsilon_0}\frac{1}{z}\Big|_{\infty}^{a}$$

$$W = -\frac{q^2}{16\pi\epsilon_0 a}$$

Now apply a similar treatment to the electron's work against the ion core…

$$W = \int_{\infty}^{a} \frac{-q^2}{4\pi\epsilon_0}\left(\frac{1}{a+z}\right)^2 dz$$

$$W = \frac{-q^2}{4\pi\epsilon_0}\int_{\infty}^{a}\left(\frac{1}{a+z}\right)^2 dz$$

$$W = \frac{q^2}{4\pi\epsilon_0}\frac{1}{a+z}\Big|_{\infty}^{a}$$

$$W = \frac{q^2}{8\pi\epsilon_0 a}$$

Adding these two contributions together yields

$$\Delta E = \frac{q^2}{16\pi\epsilon_0 a}$$

Thus, the ionization level shifts up as the ion approaches the surface.

1.3.2. Level broadening

If the ionization level retains its normal narrow shape as it approaches the metal surface, it would be expected that the ionization probability should be either zero or one; zero if the shifted ionization level is above the Fermi level, or one if it is below. This does not agree with experiment, however, as there are many experimental results that have measured intermediate values for the neutralization probability [13-16].

These intermediate neutralization probabilities arise from the broadening of the ionization level, which attains some width in energy space due to the overlap with the continuum of states in the solid. This means that there can be a state that is partially above and partially below the Fermi level. If the state has some width at the freezing distance, the ion can be partially neutralized when it arrives at the detector [17]. When measured, this partially neutralized state collapses into either a filled state or an empty state, with a probability determined by the extent of the partial neutralization.

For a crystal, the width of the broadening is determined primarily by two factors: the band structure of the solid and the perpendicular component of the exit velocity of the ion. The band structure is important because of band gaps, that is, if there are band gaps near the energy of the ionization level during scattering, they will not contribute to the overlap in electronic wave functions. The magnitude of the perpendicular velocity is important because that determines the "adiabaticity" of the scattering process. The

slower the ion, the more adiabatic the scattering will be, which translates to a longer effective freezing distance. At longer distances, there is less overlap of the wave functions, which means less broadening of the ionization level.

There have been attempts to determine the broadening of the ionization level from first principles, particularly that of Nordlander and Tully [18]. They use a "complex scaling" method to calculate the broadened energy widths of the alkali ions up to Cs. The "complex scaling" method involves rotating the wave functions into the complex plane, calculating the appropriate eigenvalues using a finite set of plane waves as a basis set, then showing that the eigenvalue's dependence on the angle of rotation into the complex plane is small. This dependence can be reduced by expanding the basis set, but they show that the dependence is sufficiently small even choosing a relatively small, and hence computationally tractable, basis set. The end result contains many parameters and has the form…

$$\Delta E_z = \frac{\Delta_0}{\left(e^{4\alpha z} + \left(\frac{\Delta_0}{\Delta_{sat}}\right)^4 - 1\right)^{1/4}}$$

These parameters must be determined for each choice of ion and substrate.

1.3.3 Neutralization from nanoclusters

Because metal nanoclusters have different electronic structure from bulk metal, their neutralization characteristics are correspondingly different. 2 keV Na^+ scattering from bulk gold, for instance, has a neutralization probability of only a few percent while Au nanoclusters supported on TiO_2 can have a neutralization probability as high as 50% [19].

This happens because quantum confined states in the clusters alter the LEP at the surface so that the electrons can more easily tunnel to the scattered ion. The difference in the neutralization is illustrated in the diagram below.

Figure 1.6 shows spectra of both total scattered yield and scattered neutrals only for two different coverages of Au on TiO_2. Small amounts of deposited Au, like the 0.5 monolayer deposition in the lower panel, yield smaller clusters, which neutralize scattered ions more efficiently. Larger amounts of deposited Au produce larger clusters or even continuous films, like the 15 monolayer deposition. These surfaces generate fewer neutrals and more multiple scattering. Note that the neutrals spectrum of the 15 monolayer Au film is scaled by a factor of 10 to make it visible.

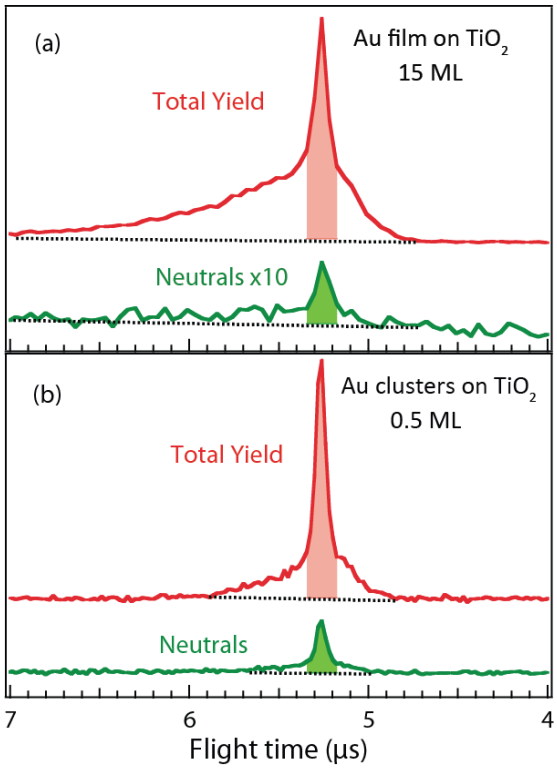

Figure 1.6 TOF-LEIS spectra of 2 keV Na^+ scattering from different amounts of Au/SiO_2

1.4 Experiment design

A specialized technique is needed to experimentally determine the neutralization probability while collecting energy spectra. The standard method of analyzing scattered ions is to use an electrostatic analyzer, which cannot detect neutral species.

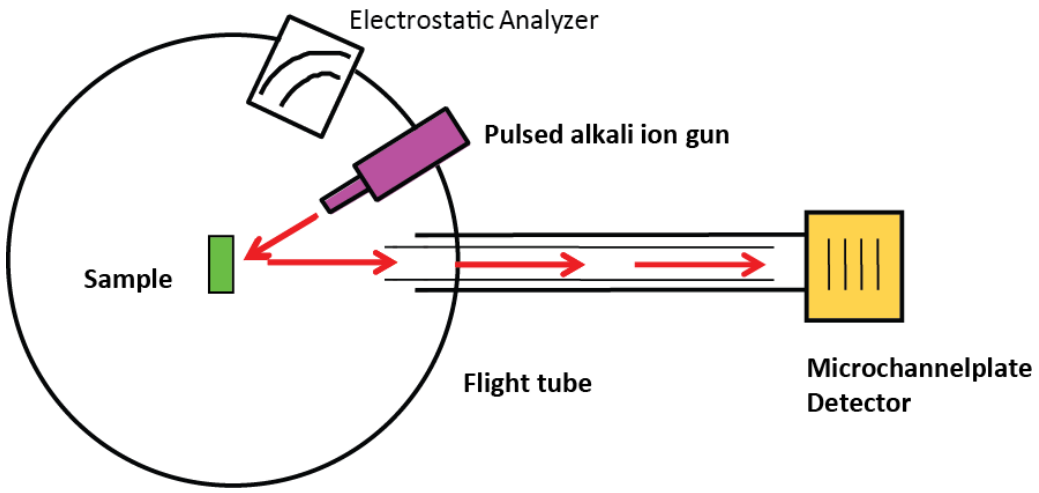

Figure 1.7 Diagram of a typical experimental setup for TOF-LEIS.

A way to collect all scattered particles independent of their charge state is to scatter directly into an electron multiplier. Our electron multiplier is an array of microchannelplates (MCPs) assembled in our lab. An MCP is a glass plate with micron-sized holes etched into it at an angle relative to the surface of the plate. When a scattered particle reaches the detector, it hits the plate and creates secondary electrons. A high voltage is applied across the plates so that the secondary electrons are pulled into the microchannels. These electrons in turn create more secondary electrons which are pulled further down into the channels. This becomes a cascade of increasing numbers of electrons until they reach the anode and are counted as a single pulse. Since the detection

efficiency depends only on the kinetic energy of the scattered particles, the front of the detector is grounded so that scattered ions and neutrals arrive with the same velocity. Finally, a pair of electrostatic deflection plates is placed in front of the detector. When grounded, the detector will see the total scattered yield. When charged, the scattered ions will be deflected away, leaving only the neutrals.

The MCP array produces pulses that can be counted to determine the total number of events. It cannot tell the difference between particles scattered from different species, background due to recoiled substrate atoms, or any other source of background. Because of this, the MCP detector is placed at the end of a ~0.65 m tube and used as part of a Time-of-Flight (TOF) spectrometer. The ion gun is pulsed at a rate of 40-80 kHz, with a rise time of about ~100 ns. The ions reach the detector in ~1 μs, so the 100 ns rise time gives sufficient resolution. A measurement is made of the time difference between a pulse of ions and an event in the detector. These events are histogrammed to create a spectrum, of either the total yield and the scattered neutrals, depending on the state of the deflection plates. Thus, the TOF spectrometer allows us to determine which events correspond to scattering from the species of interest, and the deflection plates allows us to determine the charge state of the scattered particles.

TOF spectroscopy has other advantages in addition to its use as a charge-resolved spectrometer. Beam damage is lower in a TOF experiment than during a traditional ion scattering experiment because a TOF experiment collects all scattered ions at all times. An electrostatic analyzer filters the scattered ions by energy, so the majority of the

scattered ions do not reach the detector at any given point in time. Keeping the exposure of ions on the surface low is particularly important when studying neutralization of alkali ions. In addition to worrying about beam damage, we must also worry about contaminating the surface with the beam. Alkali metals have very low work functions, so that embedded Na, for instance, can lower the surface's work function and thus change the neutral fraction. To demonstrate this point, a quick estimation of the surface contamination in a typical experiment follows.

$$n \approx A \left(\rho \frac{N_A}{\bar{m}}\right)^{2/3}$$

Here, n is the number of atoms visible to the beam, A is the cross-sectional area of the ion beam, ρ is the density of the substrate, N_A is Avogadro's number, and $\bar{m}$ is the average molar mass of the substrate. Our ion beam has a cross-sectional area of ~1 mm^2, the density of TiO_2 is 4.23 g/cm^3, and the average molar mass of a mixture one part titanium and two parts oxygen is 26.62 g/mol. Substitution yields

$$n \approx 2.1 \times 10^{13} atoms$$

We will now compare that number to the number of ions incident upon the surface. With a typical beam current of 10 pA while the beam is being pulsed, the sample is exposed to ~6.2×10^7 ions/second in the 1 mm^2 beam spot. Thus, about ~1% of the surface atoms are hit by ions in ~3400 seconds, or about one hour. Since experimental runs are likewise on the order of an hour, and in many cases even less, this is an acceptable amount of beam damage while collecting a TOF spectrum.

A typical pair of TOF spectra, with the total yield spectrum and the corresponding neutrals only spectrum, is shown below. The area corresponding to the single scattering peak (SSP) is shaded, as it is used to determine the neutral fraction. This region corresponds to ions that scatter once from a single surface atom before reaching the detector. Note, however, that the method of finding the SSP may differ from experiment to experiment. Also note that the spectra are shown with the time axis reversed, so that increasing energy is to the right, in the same manner as in a typical LEIS energy spectrum. The multiple scattering (MS) and plural scattering (PS) regions are also labeled.

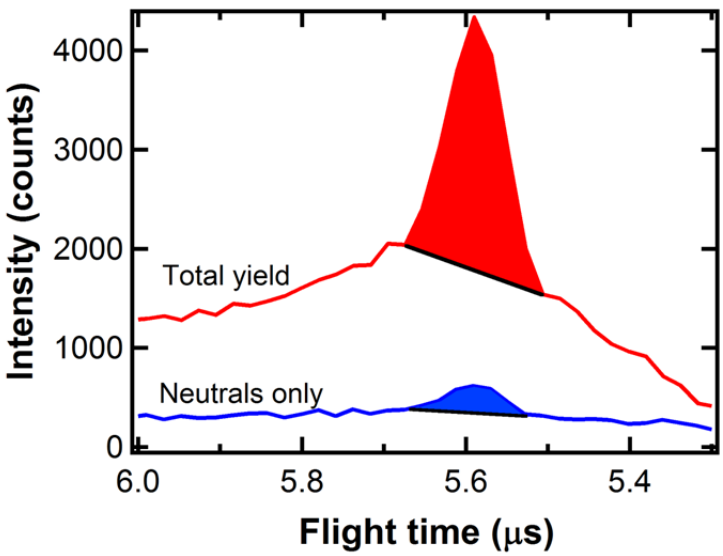

Figure 1.8 Typical total yield and neutrals only spectra with highlighted SSPs.

1.5 Data analysis

There are several options for calculating the neutralization probability, and each data set requires the selection of an appropriate method. In the simplest case, where the noise is

very small compared to the signal, the heights of the single scatting peaks could be compared. The experiments described in this thesis, however, contain considerable backgrounds that must be accounted for in a more sophisticated fashion.

The simplest method utilized in this thesis is to draw a straight line background, such as the one in Figure 1.7. The endpoints of the single scattering peaks are selected by inspection, and the trapezoid underneath constitutes the background. If the spectrum of the total yield is *T(t)*, the initial and final points of the single scattering peaks are t_1 and t_2 respectively, and the resolution of the spectrum is Δt, the number of counts in the total yield single scattering peak becomes

$$A_{tot} = \frac{1}{\Delta t}\int_{t_1}^{t_2} T(t)\, dt - \frac{T(t_2) - T(t_1)}{2}(t_2 - t_1)$$

The number of counts in the neutral single scattering peak, A_{neu}, is calculated in the same way, such that the neutralization fraction is

$$NF = \frac{A_{neu}}{A_{tot}}$$

In some cases, the background has a strongly curved shape and the signals themselves may be small. In this case, it is no longer sufficient to approximate the background as a straight line, and it becomes necessary to substitute some other function for the background. Unfortunately, there is no readily available analytical expression for the background. Thus, it becomes necessary to do a least-squares fit to the background for each spectrum. To this end, the part of the spectrum that contains scattering counts is

excluded from the fit. This too is done by inspection. If the background so calculated for the total spectrum is denoted T_b, the number of counts in the total single scattering peak is

$$A_{tot} = \frac{1}{\Delta t}\int_{t_1}^{t_2}[T(t) - T_b(t)]dt$$

1.5.1 Error analysis

An ion scattering experiment is an experiment with many trials but few successes, with a typical beam current of 10 pA (~6.2x10^7 incident ions per second) yielding about 200 detector events per second. Furthermore, some of those events may correspond to recoiled surface atoms rather than scattered ions. Thus, we have a binomial distribution with a small probability of success, and we can approximate the uncertainty in the area of our measurements as

$$\Delta A_{tot} = \sqrt{A_{tot}}$$

However, the quantity we want is the uncertainty in the neutral fraction, which is found through standard error propagation.

$$\frac{\Delta NF}{NF} = \sqrt[2]{\left(\frac{\Delta A_{tot}}{A_{tot}}\right)^2 + \left(\frac{\Delta A_{neu}}{A_{neu}}\right)^2}$$

This can lead to some underestimation of the error because it presumes that the background subtraction does not make any contribution to the uncertainty. It is sometimes preferable to calculate the uncertainty of the neutral fraction from the variance of several neutral fraction measurements. Fortunately, the resolution of the spectra is much finer than the width of the single scattering peak, so that this peak consists of many

points in the spectra. By subtracting off the background and doing a point-by-point calculation of the neutral fraction using the five points about the highest point in the single scattering peak, we can effectively get multiple simultaneous measurements of the neutral fraction without subjecting the sample to extended exposure to the scattering beam that repeated experiments would necessitate. Thus, the uncertainty becomes the standard error of the mean of the neutral fraction measurements, which is

$$\Delta NF = \frac{\sigma}{n-1} = \frac{\sigma_{NF}}{4}$$

1.6 Summary of original research

In chapter 2, we present ion scattering and work function data from Pt on TiO_2 after evaporating the metal onto the surface, then subsequently sputtering it away. It was found that SMSI can be activated by sputter beams as well as by annealing. In chapter 3, we present ion scattering data for K^+ scattering from Au on SiO_2 as a function of surface temperature, ranging from ~100 K to room temperature. It was found that the neutral fractions depend on temperature in this case, independent of any underlying structural change. In chapter 4, we present ion scattering data from Au/SiO_2 as a function of post-annealing temperature, ranging from 350 to 1000 K. It was discovered that annealing leads to inhomogeneous cluster size distributions due to static coalescence, and that this is visible to LEIS. A new way to analyze LEIS spectra and extract more useful information from them is also described.

Chapter 1 bibliography

1. X. Lai, T. P. St Clair, M. Valden, and D. W. Goodman, Prog. Surf. Sci. **59**, 25 (1998).

2. B. Bo, T. Ohkubo, and Y. Hirotsu, J. Electron Microsc. **44**, 182 (1995).

3. T. Takei, T. Akita, I. Nakamura, T. Fujitani, M. Okumura, K. Okazaki, J. H. Huang, T. Ishida, and M. Haruta, in *Advances in Catalysis, Vol 55*, edited by B. C. Gates and F. C. Jentoft (Elsevier Academic Press Inc, San Diego, 2012), Vol. 55, p. 1.

4. M. Haruta, S. Tsubota, T. Kobayashi, H. Kageyama, M. J. Genet, and B. Delmon, J. Catal. **144**, 175 (1993).

5. O. Dulub, W. Hebenstreit, and U. Diebold, Phys. Rev. Lett. **84**, 3646 (2000).

6. W. T. Wallace, B. K. Min, and D. W. Goodman, Top. Catal. **34**, 17 (2005).

7. G. Yang, W. T. Wang, Y. L. Zhou, H. B. Lu, G. Z. Yang, and Z. H. Chen, Appl. Phys. Lett. **81**, 3969 (2002).

8. T. Endo, T. Sunada, T. Sumomogi, and H. Maeta, Mater. Charact. **48**, 159 (2002).

9. C. E. J. Mitchell, A. Howard, M. Carney, and R. G. Egdell, Surf. Sci. **490**, 196 (2001).

10. S. Tauster, S. Fung, R. Baker, and J. Horsley, Science **211**, 1121 (1981).

11. F. Pesty, H. P. Steinruck, and T. E. Madey, Surf. Sci. **339**, 83 (1995).

12. A. R. Canario, T. Kravchuk, and V. A. Esaulov, New J. Phys. **8**, 227 (2006).

13. A. R. Canario and V. A. Esaulov, J. Chem. Phys. **124**, 224710 (2006).

14. H. Hamoudi, C. Dablemont, and V. A. Esaulov, Surf. Sci. **602**, 2486 (2008).

15. S. Balaz and J. A. Yarmoff, J. Phys.: Condens. Matter **22**, 084009 (6 pp.) (2010).

16. K. A. H. German, C. B. Weare, and J. A. Yarmoff, Phys. Rev. B **53**, 10407 (1996).

17. J. Los and J. J. C. Geerlings, Phys. Rep. **190**, 133 (1990).

18. P. Nordlander and J. C. Tully, Physical Review B **42**, 5564 (1990).

19. G. F. Liu, Z. Sroubek, and J. A. Yarmoff, Phys. Rev. Lett. **92**, 216801 (2004).

Chapter 2

Ion impact-induced Strong Metal Surface Interaction in $Pt/TiO_2(110)$

2.1 Introduction

Since Haruta's discovery of the catalytic activity of Au nanoclusters on oxide supports,[1] there has been much interest in the properties of supported metal nanoclusters. In addition to catalysis, these systems show promise to advance sensors, optoelectronics and other technologies. Previous studies have shown that the unique catalytic and electronic properties of metal nanoclusters on oxide supports depend on the size of the clusters.[2,3] More detailed studies of Au on TiO_2 explored the relationship between catalytic activity and cluster size using both theoretical calculations and measurements of chemical activity performed in conjunction with scanning tunneling microscopy (STM) and other surface-sensitive tools.[4,5] Subsequent studies sought to probe the electronic structure of metal nanoclusters to explain the enhanced chemical activity.[6] Although the current consensus is that particular atomic configurations around the Au nanoclusters are needed to obtain the enhanced activity,[7] the role of the cluster electronic structure in catalysis is largely unknown.

Because the local configuration around the clusters is important, interactions between these reducible oxide supports and the noble metal overlayers have important implications for the performance of catalysts. For example, the strong metal-surface interaction (SMSI) causes H_2 and CO_2 chemisorption to be dramatically reduced when systems such as Pt/TiO_2, Rh/TiO_2, and Pd/TiO_2 are annealed to 500°C in vacuum.[8]

SMSI has also been observed with other reducible oxides and other metals with high surface energies.[9] It was later suggested that the reduced chemical activity resulting from SMSI was due to the oxide support migrating on top of the metal clusters.[10,11] This encapsulation model was confirmed by Dulub, et al. via atomic resolution scanning tunneling microscope images of post-annealed Pt clusters grown on TiO_2(110), and by the disappearance of the Pt signal in He^+ ion scattering.[12] Majzik reports similar results for Rh/TiO_2.[13] In all these prior cases, encapsulation associated with SMSI was achieved by annealing.

Ion impact is another useful way to impart energy in a manner that induces the movement of surface atoms.[14] For example, low energy ion bombardment can form nanoscale periodic structures through the interplay between sputtering and surface diffusion.[15-18] Nanodots and nanowires have been produced in single material systems in this manner, with the particular structures formed being dependent on the ion energy, impact direction, etc. Under other conditions, ion bombardment can instead smooth surfaces.[19] A method of forming isolated metal nanoclusters on an oxide surface, such as would be useful for catalysis, would be to bombard a thin metal film on an oxide substrate with low energy ions. Nanostructures have been formed in this way, such as nanopatterns of Cu on SiO_2,[20] Pt on SiO_2,[21] and Cu nanowires on Si and glass.[22] In addition, Rh surfaces patterned by ion beam sputtering have been shown to be effective in inducing the dissociation of CO.[23]

In previous work, we used the neutralization of backscattered alkali ions during Low Energy Ion Scattering (LEIS) as a probe of the electronic structure of Au

nanoclusters. The extent of the neutralization of scattered alkalis, which occurs via a resonant charge transfer process, provides information on the local electronic properties at the scattering site.[24,25] We showed that small nanoclusters, grown by direct deposition of Au metal onto an oxide substrate, neutralize scattered alkali ions more efficiently than the bulk material.[2,6,26,27] It was proposed that the nanoclusters have filled states that provide charge to enable the additional neutralization, making this a unique and sensitive technique for identification of the local electronic properties of metal nanoclusters. Note that there are no other tools readily available that can be used for the direct identification of such states. LEIS has the additional advantage that it can be deployed for studies of rough materials, such as those produced by ion bombardment, unlike techniques such as STM.

Additional experiments showed that enhanced neutralization is also observed after bombarding a thin Au film grown on TiO_2 with a sufficiently large fluence of low energy Ar^+.[28] This suggests that ion bombardment does not merely sputter away the metal, but also forms nanoclusters that are electronically similar to those produced by deposition. This result provided strong evidence that the fabrication of useful catalysts is possible via ion bombardment of a thin metal film deposited on an insulating substrate. Such a process may be scalable for industrial applications.

The present work started as an attempt to expand this method to Pt/TiO_2. It was presumed to first order that the cluster formation is solely a consequence of the ion bombardment kinematics, so that similar behavior was expected. This is, however, not the case for bombarded Pt/TiO_2. Instead, it is shown that SMSI, facilitated by the ion

beam, hinders the formation of nanoclusters when bombarding a thin Pt film. The absence of enhanced neutralization for a sputtered Pt film is attributed to an ion-induced interaction of substrate material with the clusters. This, to our knowledge, is the first report of an ion-induced encapsulation of surface species. This has implications for ion-beam processing of materials, in general, and also suggests a novel means for the production of coated nanoparticles.

2.2 Experimental procedure

The experiments were carried out in an ultra-high vacuum (UHV) chamber with a base pressure below $5x10^{-10}$ torr. Initial *in situ* sample preparation involved repeated cycles of sputtering and annealing an 8 mm x 8 mm polished rutile $TiO_2(110)$ single crystal (Commercial Crystal Laboratories). 500 eV Ar^+ ions at a current of 2 μA in a 13 mm^2 spot size were used to sputter the sample for a total of 5 minutes to remove surface contaminants. During sputtering, the sample was periodically moved along the x and y planes to ensure that the entire wafer was exposed to the beam uniformly. Following sputtering, the samples were recrystallized by annealing at 900 K for 5 minutes in UHV. Cleanliness of the $TiO_2(110)$ substrate was verified by Auger Electron Spectroscopy (AES), and crystalline order was verified by observation of a sharp 1x1 pattern with Low Energy Electron Diffraction (LEED).

Pt was evaporated from a tungsten filament (Mathis) wrapped with high-purity wire (99.9% Pt). The deposition rate was calibrated using a quartz crystal microbalance. After an 87 Å Pt thin film was grown, it was sputtered stepwise by bombarding the surface with Ar^+ in the same manner as used for the initial cleaning.

The change in surface work function was monitored following each deposition of Pt and subsequent ion bombardment cycle of the Pt film. Changes in the work function were determined by exposing the sample to 1 keV electrons while collecting a spectrum of the emitted secondary electrons employing the LEED optics as in ref. [29]. The movement of the secondary electron cutoff reflects any changes in the surface work function.

LEIS time-of-flight (TOF) spectra were collected using incident 2.5 keV Na^+ ions as described previously[26] and summarized here. A modified Kimball Physics IGS-4 alkali ion gun produces approximately 50 pA in a 3 mm^2 spot. The beam is pulsed at 80 kHz with a width of approximately 100 ns. The projectiles are directed to the sample at a 30° angle from the normal, and those that exit along the sample normal are collected by the detector, i.e., the scattering angle is 150°. The scattered particles are collected by a triple micro-channelplate detector located at the end of a 0.65 m flight tube. The front of the detector is held at ground potential to insure the neutrals and ions impact with the same kinetic energy, and hence have the same detection efficiency.[30,31] The time differences between the incident ions impacting the sample and the scattered projectiles reaching the detector are histogrammed to produce a TOF spectrum. Deflection plates in the flight tube separate scattered ions from neutrals, allowing for the independent collection of spectra for the total scattered yield and the scattered neutrals. The total yield and neutral spectra are collected simultaneously, rather than sequentially, by switching the deflection plates on and off every minute, which eliminates inaccuracies that would result from long-term drifts in the incident ion beam current. Collecting a spectrum with

reasonable statistics takes between 20 minutes and 2 hours, depending on the Pt coverage.

2.3 Results

Figure 2.1 shows representative "total yield" and "neutrals only" time-of-flight (TOF) spectra for 2.5 keV Na^+ ions scattered from 87 Å of Pt deposited on TiO_2(110). These spectra are typical, in terms of the spectral features, of those collected following all depositions greater than 4 Å. Note that the time scale in the figure is reversed so that increasing energy of the scattered projectiles is towards the right. The most prominent feature in the spectra is the single scattering peak (SSP). The SSP corresponds to projectiles that experience a single hard collision with a surface Pt atom and backscatter directly into the detector.[32] To the right of the SSP (shorter time, higher energy) is the plural scattering (PS) region, which represents projectiles that experience two or more in-plane scattering events in which the projectile overall loses less energy than it would in a single collision at the same scattering angle.[33] To the left of the SSP (longer time, lower energy) is the multiple scattering (MS) region, which represents projectiles that experience two or more out-of-plane scattering events. Background subtraction and integration of the SSPs, as illustrated in Fig. 2.1, allows for a determination of the neutral fraction (NF) by dividing the area of the neutral SSP by that of the total yield SSP employing a similar procedure as described in refs. [26] and [34].

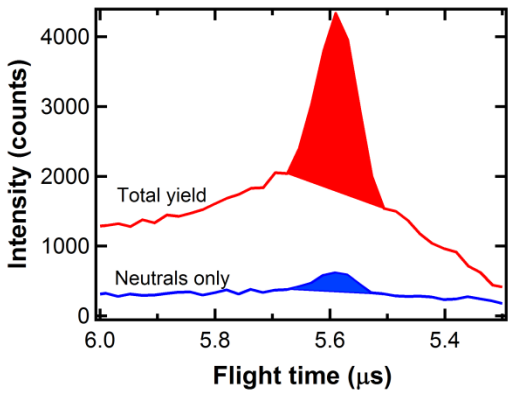

Figure 2.1. Representative "total yield" and "neutrals only" TOF spectra for 2.5 keV Na^+ scattered from 87 Å of Pt deposited on TiO_2(110).

Note that Na^+ is used as the projectile because it is relatively heavy and will backscatter from the more massive Pt atoms, but not from the lighter Ti or O atoms. Should a Na projectile pass through a Pt nanocluster and interact with a Ti or O atom, it would then scatter in the forward direction becoming embedded in the crystal and no longer able to backscatter from the sample. Thus, Na^+ projectiles enable the clusters to be probed without any background signal from the substrate.

Figure 2.2 shows raw total yield TOF spectra collected following a range of Pt depositions onto TiO_2. The SSP is the dominant feature in all of the spectra, and its intensity and the relative contributions from MS and PS scattering events initially increase with Pt coverage.

The structure of the deposited Pt is reflected by the MS and PS contributions to the TOF spectra. Such features will appear when large enough 3D structures are present to enable multiple collisions from nearby heavy atoms that still lead to backscattering at energies close to that of the SSP.[27] Because 3D clusters of Pt are formed very quickly, PS and MS features are expected to appear in Pt/TiO_2 at very low coverages, and such

features are present following the initial 1 Å coverage. The proportion of multiple scattering increases with additional coverage, since the possibility for multiple and plural scattering within a single Pt cluster also increases as the size of the clusters increases. Close inspection shows that the relative contribution of MS and PS features saturates by about 4 Å, which is reasonable once the size of the Pt clusters is comparable to the average distance from the initial impact site that the scattered projectiles probe.

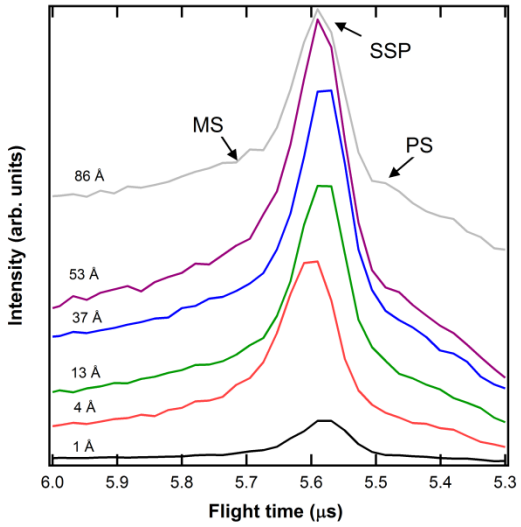

Figure 2.2: Raw total yield 2.5 keV Na^+ TOF spectra collected from Pt grown on TiO_2 at the coverages indicated. The spectra are shown as absolute intensities, but offset for clarity.

Figure 2.3 shows the raw total yield spectra collected from a 87 Å Pt film deposited onto TiO_2(110) and following various fluences of 500 eV Ar^+ sputtering. As the ion fluence passes beyond about $2x10^{16}$ cm^{-2}, the SSP attenuates and broadens while the MS features become less distinct because the overall relative intensity on the low energy side of the SSP increases. The reduction in the size of the SSP is evidence that the amount of Pt on the surface is reduced with sputtering, while the persistence of the MS

and PS features indicates that the Pt is still clustered even after sputtering. The fact that the SSP is visible after sputtering demonstrates that at least some of the Pt is still exposed at the surface.

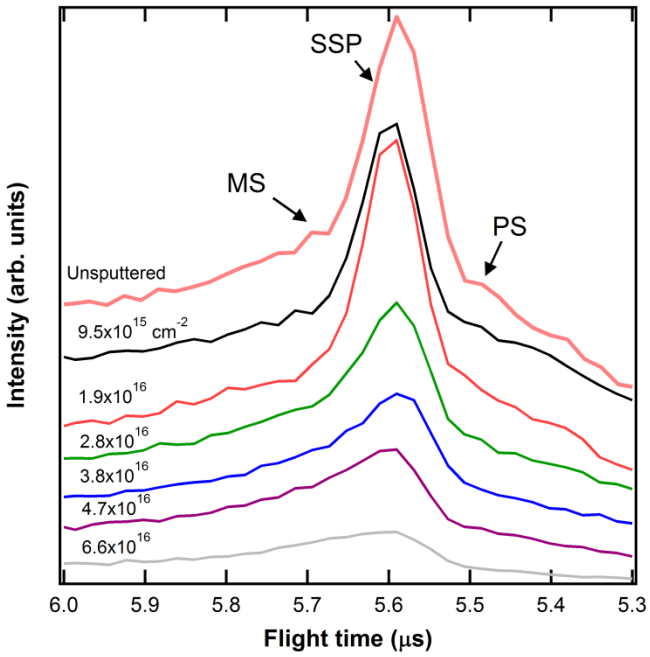

Figure 2.3: Total yield 2.5 keV Na^+ TOF spectra collected from a sputtered 87 Å Pt thin film on TiO_2. The Ar^+ sputtering fluences are indicated in the figure. The spectra are shown as absolute intensities, but offset for clarity.

The top panel of Fig. 2.4 shows the NF for scattered Na^+ as a function of the amount of Pt deposited. The NF is 0.32 following the initial deposition of 1 Å of Pt, and it decreases to about 0.07 as the coverage approaches 40 Å. The uncertainty in each reported NF is assumed to be solely the result of shot noise, and is often less than the size of the symbols. Additional runs of this experiment are not shown, but the results are comparable. A decrease in NF with cluster size is qualitatively the same behavior as was observed for Au[6,26] and Ag[2] on TiO_2(110) and for Au on partially oxidized Si and SiO_2.[27]

The surface work function increases quickly with Pt deposition by about 0.35 eV for a 10 Å thick film, as shown in the bottom panel of Fig. 2.4, and does not change with further deposition. The work function of clean TiO_2(110) is reported to be 4.2 eV,[35] while that of polycrystalline Pt is 5.65 eV.[36] Interestingly, even though this difference is on the order of 1.45 eV, the change between rutile TiO_2(110) and a thin film of Pt on TiO_2(110) is reported to be only 0.4 eV,[37] consistent with our results.

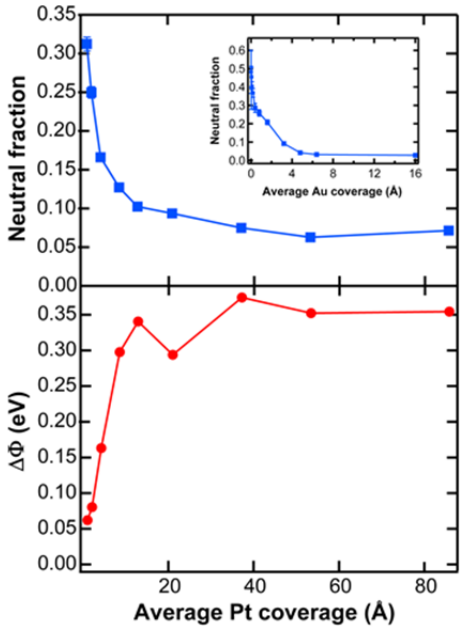

Figure 2.4: Neutral fraction (top panel) and work function shift (bottom panel) as a function of Pt film thickness. The inset shows similar neutral fraction data for Au/TiO_2 taken from ref. [6].

Larger depositions generally correspond to larger nanostructures[38-40] until sufficient Pt is deposited to form a complete film. Thus, in the initial part of Fig. 2.4 the x-axis is a reflection of the cluster size, although the relationship is not linear. The NF and work function both stop changing when the coverage reaches about 20Å, which is

also beyond the point at which the shapes of the TOF spectra have stabilized. Thus, this coverage likely corresponds to the point at which a complete film is just formed.

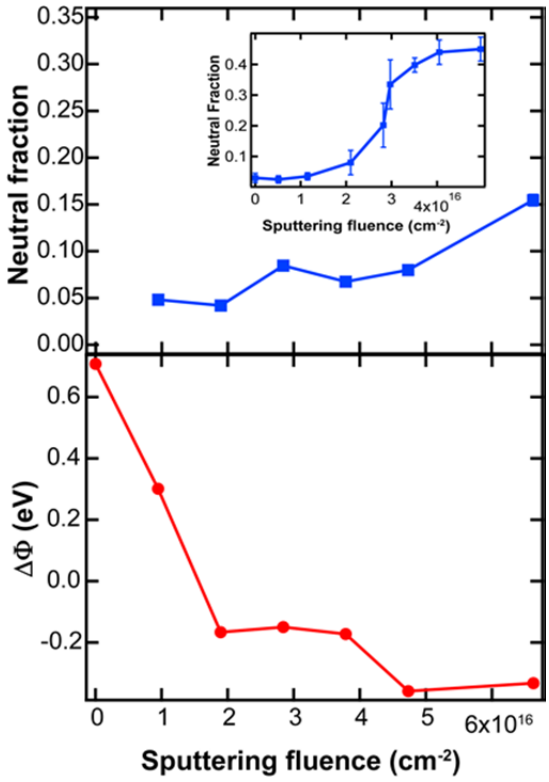

Figure 2.5: Work function shift and neutral fraction collected from an 87 Å Pt thin film on TiO_2(110) as a function of fluence for 500 eV Ar^+ ion bombardment. The inset shows similar data for a 150 Å Au film on TiO_2 taken from ref. [28].

Figure 2.5 shows the NF and work function data for the 87 Å Pt thin film as a function of 500 eV Ar^+ ion bombardment. The NF starts at 0.07 and is fairly insensitive to the ion bombardment, although it rises slightly towards the end of the measurement to about 0.15. The work function decreases rapidly with the initial sputtering, dropping below the clean TiO_2 surface value and plateauing around -0.3 eV. Note that the work function is larger at the beginning of the ion bombardment than it was at the end of the growth of the thin film. This increase could be due to adsorption of small amounts of

background gases after leaving the sample overnight in vacuum following the film growth, although AES showed no evidence of contamination. The work function does decrease quickly with ion bombardment, however, which may correspond to a rapid removal of adsorbed contaminants. Whatever the cause of the small change to the pre-bombardment work function, it is clear that that the NF is largely unchanged by Ar^+ ion bombardment while the work function decreases significantly.

For comparison, the insets to Figs. 2.4 and 2.5 show data for growth and ion bombardment of Au/TiO_2 taken from earlier measurements.[6,28] When depositing Au onto clean TiO_2(110), the NFs behave qualitatively similar as in scattering from deposited Pt, although the magnitudes are greater with Au. When a 150 Å Au film is sputtered by 500 eV Ar^+, however, the NF increases abruptly after a threshold fluence to roughly the same value as the small clusters formed upon deposition. This is in stark contrast to the behavior of ion bombarded Pt/TiO_2.

2.4 Discussion

Charge exchange during alkali ion backscattering is well described by the Resonant Charge Transfer (RCT) model.[41] When an alkali ion approaches a surface, its ionization level shifts upward because of the image charge and simultaneously broadens due to the overlap between the level and states in the surface. The interaction time during the scattering is comparable to the electron tunneling rate, however, so that the neutralization occurs non-adiabatically. The probability for neutralization depends on the overlap between filled states in the surface and the broadened and shifted ionization level when the projectile is at an effective "freezing distance" above the surface. Because

the process is non-adiabatic, this distance depends on the projectile velocity, among other factors, and is typically on the order of a few angstroms.[42] A consequence of RCT is that when the work function is reduced, the neutralization probability increases, and vice versa. When scattering from a traditional solid, the NF is largely determined by the local work function just above the scattering site.[24,25]

When scattering from Au nanoclusters, however, the neutralization probability is larger than what would be predicted by a simple RCT model involving a normal metallic solid.[6,27] To explain this, it was proposed that electrons in negatively charged quantum-confined states in the nanoclusters provide the extra charge by coupling directly to the ionization level during scattering. Simulations[43] and Kelvin probe force microscopy[44] have indicated that Au clusters on TiO_2 are indeed negatively charged, providing further support for this interpretation.

As shown by STM studies,[39] Pt evaporated onto TiO_2 forms 3D clusters at coverages as low as 0.25 Å. These clusters have an average diameter of 14 Å when the average Pt coverage is 0.76 Å.[45] As more Pt is added, the clusters increase in size and coarsen, and eventually a thin film develops. This is different from the behavior of Au on TiO_2, where experiments show that 2D islands initially develop,[46] followed by 3D clusters, and finally a thin film. Because Pt forms clusters upon deposition, the electrons in the Pt clusters may be confined in a similar manner as for Au, resulting in higher neutral fractions than would be expected simply from the work function of bulk Pt.

Pt and Au are electronically similar noble metal materials with many *d* and *f* electrons and their surface work functions are both relatively high compared to most

metal surfaces. Because of this, it might be expected that similar neutralization would result after scattering from either one. Indeed, the small Pt nanoclusters grown on TiO_2 by deposition do neutralize Na^+ more efficiently than the bulk-like Pt film, suggesting that they are negatively charged in a similar manner as Au nanoclusters. The magnitudes of the NFs are overall smaller for Pt, but this is consistent with the RCT model since Pt generally has a larger work function than Au.

Despite the apparent similarities of Au and Pt, however, they have different chemistry. For example, bulk Pt catalyzes CO oxidation at room temperature while bulk Au does not.[47] Evidence of chemical differences in nanoclusters of Pt and Au is borne out by the measured NFs, which do not become enhanced when sputtering a Pt/TiO_2 thin film. Since the Pt film used in this work is thinner than the Au film used to generate the inset to Fig. 2.5[28] and a larger ion fluence was used, an enhanced NF would have been observed under these conditions if the Au and Pt systems were comparable. The fact that the NF was not restored by ion bombardment therefore indicates that the structure of the sputtered Pt film is different from that of Pt nanoclusters formed by deposition, and this difference is fundamentally chemical in nature.

Taken together, the growth and sputtering experiments provide strong evidence that the neutralization in scattering from Pt clusters is not primarily dependent on the surface work function. If that were the case, the NF and work function changes would be correlated during the sputtering experiment (Fig. 2.5), and they clearly are not. Instead, the work function is restored to the clean surface value by as little as $1x10^{16}$ cm^{-2}, but the NF does not rise at the same time. Indeed, the NF never rises to the 0.30 value seen

following small depositions of Pt though the work function decreases even beyond its initial value.

Since Au/TiO_2 does not exhibit the SMSI effect[42] while Pt/TiO_2 does,[8,9,12] it is reasonable to propose that the relative insensitivity of the Pt NF to ion bombardment is a consequence of SMSI. Although our samples are held at room temperature during bombardment, which would not ordinarily lead to encapsulation, the Ar^+ ions can provide sufficient energy to enable diffusion of the substrate material. Thus, TiO_2 from the substrate would have enough mobility to interact with any Pt clusters that may form as the thin film is bombarded. Although this does not appear to be a total encapsulation, as there are still plenty of Pt atoms visible to the incoming Na^+ ion beam, the NF's can still be affected by a chemical interaction between TiO_2 and Pt.

The ion-induced interaction is likely to be generated during the collision cascade created when a low energy Ar^+ ion impacts the surface.[48] The impact imparts kinetic energy to surface and near-surface atoms[49] and could facilitate diffusion of Ti and O species into the low energy configuration favored by SMSI. The notion that the kinetic energy of low energy ions can drive a system towards a thermodynamically stable configuration is not a new idea, and is supported, for example, by a study of Mo/Si multilayers prepared with and without the assistance of 200 eV ions.[50]

There are at least two ways in which such an interaction could lead to the insensitivity of the NF to sputtering. Even if the clusters do form, the TiO_2 material could be in a configuration that alters the electronic structure by withdrawing charge from the clusters, which would then reduce the NF. Although it is unlikely that the TiO_2

completely covers the Pt as it did in ref. [12], since Pt is always visible to the Na^+ ion beam, the interaction associated with even a partial encapsulation could still induce sufficient charge transfer from the clusters to significantly alter their electronic properties and achieve such a result. Alternatively, it is possible that the interaction affects the kinematics of the nanocluster formation process itself, perhaps by impeding the ability of Pt to diffuse across the surface, so that the clusters never actually form during ion bombardment as they do with Au/TiO_2.

Procedure	Neutral Fraction
Cleaned, Deposited	0.30 ± 0.01
Annealed 200°C	0.29 ± 0.01
Annealed 700°C, 500°C	0.22 ± 0.01

Table 2.1. Neutral fractions for 2.5 keV Na^+ scattered from $Pt/TiO_2(110)$ before and after annealing, as described in the text.

To test the notion that such a chemical interaction is responsible for the insensitivity of the NF to ion bombardment, the Pt clusters were purposely encapsulated by following the recipe from ref. [12], while measuring the NFs after each step, as summarized in Table 1. First, a small enough amount of Pt was deposited so that the enhanced neutralization is apparent, resulting in a NF of 0.30. Following the recipe, the surface was then annealed to 200°C for 30 minutes, which is not sufficient to induce encapsulation, and the NF was 0.29, or basically unchanged. To induce at least a partial encapsulation, the surface was next annealed to 700°C for 5 minutes and then to 500°C for 30 minutes. The NF in scattering from Pt in the partially encapsulated clusters was

0.22, which is a significant decrease. Thus, the NF is sensitive to the effects associated with encapsulation, supporting the idea that any clusters produced by sputtering the Pt film are interacting with substrate material more so than they would in the absence of SMSI.

Note that such an interaction would also explain why Pt could not be completely removed from TiO_2(110) by sputtering, as evidenced by the persistence of the Pt peak in the TOF spectra even after prolonged Ar^+ bombardment. After most of the Pt is removed, and despite the mass difference between Ar and the TiO_2 material, the encapsulating TiO_2 could lead to collisions that effectively reduce the direct impacts that Ar^+ ions have with the remaining Pt atoms, thus shielding them from being completely sputtered away. Even as some of the TiO_2 covering the Pt is removed by continuous sputtering, other atoms from the surrounding lattice would be energized by the collision cascade and take their place. Thus, there would be a quasi-steady state in which TiO_2 is removed and replaced at the same rate, while some Pt always remains just below the surface.

There is also evidence for encapsulation in the shapes of the TOF spectra themselves, as seen in Fig. 2.3. As the sputtering fluence increases, the SSP broadens. Classical mechanics effectively predicts the kinetic energy of the scattered ions after a single collision, so the shape of the SSP should not be different following sputtering. If partial encapsulation were occurring, however, then trajectories that lead to scattering at energies close to the SSP could be altered by grazing collisions with atoms in the TiO_2 film. Thus, when a Na^+ ion penetrates below the outermost surface layers and

backscatters from a Pt atom, it loses additional energy along the way resulting in a broadening of the SSP.

2.5 Conclusions

The neutralization in scattering from small clusters is enhanced relative to scattering from bulk Pt, which demonstrates that Pt deposited onto TiO_2 forms negatively charged clusters in a similar manner as Au on TiO_2.[6] This enhancement is related to the electronic properties of the nanoclusters, and is not caused simply by changes in the surface work function.

When bombarding a thin Pt film, the formation of nanoclusters is expected from the kinematics of the collision process, as demonstrated previously for Au.[28] The energy deposited by the ions leads to movement of substrate material, however, so that a partial encapsulation of any Pt nanoclusters by TiO_2 occurs due to SMSI. The oxide material in proximity to the nanoclusters withdraws charge from them, thus lowering the neutral fraction, or it could possibly act to impede the cluster formation process itself. Such an ion-driven process clearly depends on the chemical properties of the materials involved. Ion-induced encapsulation could be a useful phenomenon for the production of novel multicomponent material systems.

Further work remains to be done in probing the structure of the Pt clusters themselves, especially in the regime where the TiO_2 encapsulation occurs. Performing LEIS measurements as a function of angle, and including Monte Carlo simulations of the ion scattering spectra,[51-53] would help to address these questions.

Chapter 2 bibliography

1. M. Haruta, S. Tsubota, T. Kobayashi, H. Kageyama, M. J. Genet, and B. Delmon, J. Catal. **144**, 175 (1993).
2. A. R. Canario and V. A. Esaulov, J. Chem. Phys. **124**, 224710 (2006).
3. M. Valden, X. Lai, and D. W. Goodman, Science **281**, 1647 (1998).
4. M. S. Chen and D. W. Goodman, Catal. Today **111**, 22 (2006).
5. S. Chretien, S. K. Buratto, and H. Metiu, Curr. Opin. Solid State Mat. Sci. **11**, 62 (2007).
6. G. F. Liu, Z. Sroubek, and J. A. Yarmoff, Phys. Rev. Lett. **92**, 216801 (2004).
7. I. X. Green, W. J. Tang, M. Neurock, and J. T. Yates, Science **333**, 736 (2011).
8. S. Tauster, S. Fung, R. Baker, and J. Horsley, Science **211**, 1121 (1981).
9. Q. Fu and T. Wagner, Surf. Sci. Rep. **62**, 431 (2007).
10. D. N. Belton, Y. M. Sun, and J. M. White, J. Am. Chem. Soc. **106**, 3059 (1984).
11. Q. Fu, T. Wagner, S. Olliges, and H. Carstanjen, J. Phys. Chem. B **109**, 944 (2005).
12. O. Dulub, W. Hebenstreit, and U. Diebold, Phys. Rev. Lett. **84**, 3646 (2000).
13. Z. Majzik, N. Balázs, and A. Berkó, J. Phys. Chem. C **115**, 9535 (2011).
14. L. Hanley and S. B. Sinnott, Surf. Sci. **500**, 500 (2002).
15. R. M. Bradley and J. M. E. Harper, J. Vac. Sci. Technol. A **6**, 2390 (1988).
16. E. Chason and W. Chan, Top. Appl. Phys. **116**, 53 (2010).
17. A. Keller and S. Facsko, Materials **3**, 4811 (2010).
18. P. Karmakar and D. Ghose, Surf. Sci. **554**, L101 (2004).

19. F. Frost, R. Fechner, B. Ziberi, J. Vollner, D. Flamm, and A. Schindler, J. Phys-Condens. Mat. **21** (2009).

20. M. Stepanova and S. K. Dew, Appl. Phys. Lett. **86**, 073112 (2005).

21. X. Y. Hu, D. G. Cahill, and R. S. Averback, J. Appl. Phys. **89**, 7777 (2001).

22. M. Stepanova and S. K. Dew, J. Vac. Sci. Technol. B **24**, 592 (2006).

23. F. Buatier de Mongeot and U. Valbusa, J. Phys: Condens. Mat. **21**, 224022 (2009).

24. J. A. Yarmoff, Y. Yang, and Z. Sroubek, Phys. Rev. Lett. **91**, 086104 (2003).

25. C. B. Weare, K. A. H. German, and J. A. Yarmoff, Phys. Rev. B **52**, 2066 (1995).

26. G. F. Liu, Z. Sroubek, P. Karmakar, and J. A. Yarmoff, J. Chem. Phys. **125**, 054715 (2006).

27. S. Balaz and J. A. Yarmoff, Surf. Sci. **605**, 675 (2010).

28. P. Karmakar, G. F. Liu, Z. Sroubek, and J. A. Yarmoff, Phys. Rev. Lett. **98**, 215502 (2007).

29. C. Haque and J. Fritz, Rev. Sci. Instr. **44**, 394 (1973).

30. M. Barat, J. C. Brenot, J. A. Fayeton, and Y. J. Picard, Rev. Sci. Instrum. **75**, 2050 (2000).

31. B. Peko and T. Stephen, Nucl. Instrum. Meth. B **171**, 597 (2000).

32. H. Niehus, W. Heiland, and E. Taglauer, Surf. Sci. Rep. **17**, 213 (1993).

33. M. Draxler, R. Beikler, E. Taglauer, K. Schmid, R. Gruber, S. N. Ermolov, and P. Bauer, Phys. Rev. A **68**, 022901 (2003).

34. C. B. Weare and J. A. Yarmoff, Surf. Sci. **348**, 359 (1996).

35. A. Imanishi, E. Tsuji, and Y. Nakato, J. Phys. Chem. C **111**, 2128 (2007).

36. W. M. Haynes, *Handbook of Chemistry and Physics, 91st edition* (CRC Press, Boca Raton, 2010).

37. K. D. Schierbaum, S. Fischer, M. C. Torquemada, J. L. d. Segovia, E. Román, and J. A. Martin-Gago, Surf. Sci. **345**, 261 (1996).

38. C. T. Campbell, Surf. Sci. Rep. **27**, 1 (1997).

39. S. Gan, Y. Liang, D. R. Baer, M. R. Sievers, G. S. Herman, and C. H. F. Peden, J. Phys. Chem. B **105**, 2412 (2001).

40. X. Lai, T. P. S. Clair, M. Valden, and D. W. Goodman, Prog. Surf. Sci. **59**, 25 (1998).

41. J. Los and J. J. C. Geerlings, Phys. Rep. **190**, 133 (1990).

42. F. Cosandey, L. Zhang, and T. E. Madey, Surf. Sci. **474**, 1 (2001).

43. A. Sanchez, S. Abbet, U. Heiz, W.-D. Schneider, H. Häkkinen, R. N. Barnett, and U. Landman, J. Phys. Chem. A **103**, 9573 (1999).

44. H. J. Chung, A. Yurtsever, Y. Sugimoto, M. Abe, and S. Morita, Appl. Phys. Lett. **99**, 123102 (2011).

45. S. Gan, Y. Liang, D. R. Baer, and A. W. Grant, Surf. Sci. **475**, 159 (2001).

46. L. Zhang, F. Cosandey, R. Persaud, and T. E. Madey, Surf. Sci. **439**, 73 (1999).

47. T. V. Choudhary and D. W. Goodman, Top. Catal. **21**, 25 (2002).

48. P. Sigmund, Nucl. Instrum. Meth. B **27**, 1 (1987).

49. G. Carter, B. Navinšek, and J. L. Whitton, Top. Appl. Phys. **52**, 231 (1983).

50. E. N. Zubarev, V. V. Kondratenko, V. A. Sevryukova, S. A. Yulin, T. Feigl, and N. Kaiser, Appl. Phys. A **90**, 705 (2008).

51. V. Ignatova, D. Karpuzov, I. Chakarov, and I. Katardjiev, Prog. Surf. Sci. **81**, 247 (2006).

52. M. A. Karolewski, Nucl. Instrum. Meth. B **230**, 402 (2005).

53. J. A. Yarmoff and R. S. Williams, Surf. Sci. **127**, 461 (1983).

Chapter 3

Temperature Dependence of the Neutralization of Low Energy K^+ Ions Scattered from Au Nanoclusters on SiO_2

3.1 Introduction

Supported metal nanoclusters on oxide surfaces have potential applications in catalysis [1], optoelectronics [2], and sensors [3]. The properties of these systems are heavily dependent on their morphologies, with small nanoclusters exhibiting very different behavior than larger clusters or the bulk metal [4]. To optimize the properties of nanoclusters, there is an ongoing search for fabrication methods that provide control of their morphologies. Chemical synthesis of nanoclusters [5] is the best established method for nanocluster fabrication. Other methods being explored include the direct production of nanoclusters by Physical Vapor Deposition (PVD) [6], Buffer Layer Assisted Growth (BLAG) [7,8] and the use of low energy ions to pattern materials at the nanoscale [9,10]. Metal clusters for fundamental surface studies are most often produced using direct deposition via PVD [11,12]. Clusters form during direct deposition as a consequence of surface energy or lattice mismatch.

In this paper, we use neutralization during low energy alkali ion scattering to explore the temperature dependence of the electronic structure of gold (Au) clusters grown by PVD onto silicon dioxide (SiO_2) films. The data suggests that the cluster morphologies are unchanged within the temperature range explored, although the electronic structure changes in unexpected ways. An advantage to the use of ion scattering to interrogate nanoclusters is that the surfaces do not need to be particularly

uniform or well ordered, as is necessary for other surface analysis techniques such as scanning tunneling microscopy (STM). Furthermore, ion scattering can be carried out quickly over a wide range of surface temperatures. In order to effectively use ion scattering as a surface probe, however, the effects that surface temperature have on the neutralization probability must be well understood.

Previous experiments conducted at room temperature demonstrate that the neutralization probability of scattered low energy alkali ions is a function of the cluster size [11,13,14]. The enhanced neutralization observed with very small clusters is driven by occupied local states that lead to negatively charged nanoclusters. Within the resonant charge transfer (RCT) model normally used to describe the neutralization of scattered alkali ions [15], an increase in temperature would be expected to result in, at most, a small increase in the neutralization probability [16]. We find, however, that the neutralization decreases with temperature in a reversible manner. The implications of this unexpected behavior, and suggestions for experiments that can help to determine the underlying physics, are discussed below.

3.2 Experimental Procedure

The experiments were carried out in an ultra-high vacuum (UHV) chamber with a base pressure of 2×10^{-9} Torr. This relatively high pressure is due to the fact that the chamber was recently used for experiments involving water adsorption. Nevertheless, it can be shown that contamination is not a problem in these experiments, largely due to the inertness of SiO_2.

The Si(111) samples were mounted onto a commercial button heater (Heatwave) that was attached to a cryostat (Helitran). A clean surface was prepared *in situ* by sputtering with 500 eV Ar^+ ions following by annealing at 1173 K for 5 minutes to restore the crystallinity. A thin SiO_2 film was produced by heating the surface to 973 K for 25 minutes in 10^{-5} Torr of dry oxygen (O_2), which was continuously flowing into a turbomolecular pump to maintain purity [17]. After oxidation, the surface was allowed to cool to 550 K before evacuation of O_2 to prevent the formation of pinholes in the oxide layer [18].

The cryostat was filled with liquid nitrogen to bring the sample temperature down to 115 K prior to Au deposition. Gold wire (99.98%) was evaporated from a tungsten filament (Mathis). The evaporation rate was calibrated with a quartz crystal microbalance.

Charge-state resolved time-of-flight (TOF) spectra for the scattering of 2.5 keV K^+ were collected, as described previously [19,20], from the Au nanoclusters grown on SiO_2/Si(111) by PVD. The K^+ ions are produced from a thermionic emitter ion gun (Kimball Physics). The beam is pulsed at 80 kHz by deflection across a 1 mm diameter aperture mounted at the end of the gun to produce a pulse width of approximately 100 ns. The particles are scattered into a 0.67 m long flight tube mounted at a scattering angle of 135°. The ions are collected in a dual microchannel plate (MCP) detector at the end of the tube, with the MCP entrance held at ground potential so that the neutrals and the ions arrive with the same velocity and thus have the same detection efficiency [21]. The time differences between the K^+ beam pulses and the scattered projectile arrivals at the

detector are histogrammed to produce the TOF spectra. A pair of electrostatic deflection plates in the flight tube allows the scattered ions to be removed so that neutrals-only spectra can be collected. The collection of total yield and neutrals spectra is alternated every minute to minimize the effects of long-term drift in the incident ion beam current. A complete set of total yield and neutrals spectra is collected over a two-hour period to ensure sufficient statistics. Note that the ion beam fluence in this case is not sufficient to lead to any measurable beam damage.

3.3 Results

Figure 3.1 shows raw TOF spectra collected from 0.5 Å of Au deposited on SiO_2/Si(111) at 115 K and after raising the temperature to 360 K. The upper traces in each panel indicate the total yield, while the lower curves show the scattered neutrals. The sharp feature in each spectrum is the single scattering peak (SSP) [22]. The SSP corresponds to an ion that experiences a single binary elastic collision with a surface Au atom and subsequently backscatters directly into the detector. K^+ projectiles are used in this experiment because their relatively large mass precludes backscattering from the lighter substrate atoms, since large angle scattering only occurs when a projectile impacts a more massive target atom. When K^+ interacts with a lighter Si or O atom, it can only scatter in the forward direction, either missing the detector or becoming embedded in the substrate, and would thus not contribute to the SSP. Thus, K^+ backscattering occurs easily from Au nanoclusters, while the substrate contributes little to the spectrum. The background underneath the SSP represents a combination of multiply scattered K^+ projectiles and recoiled light surface species, such as O or H. The recoiled species

emanate from the oxide and from adsorbed water or other lightly bound contaminants. The background is reduced at the higher temperature, as presumably most of the lightly bound species are thermally desorbed before the temperature reaches 360 K.

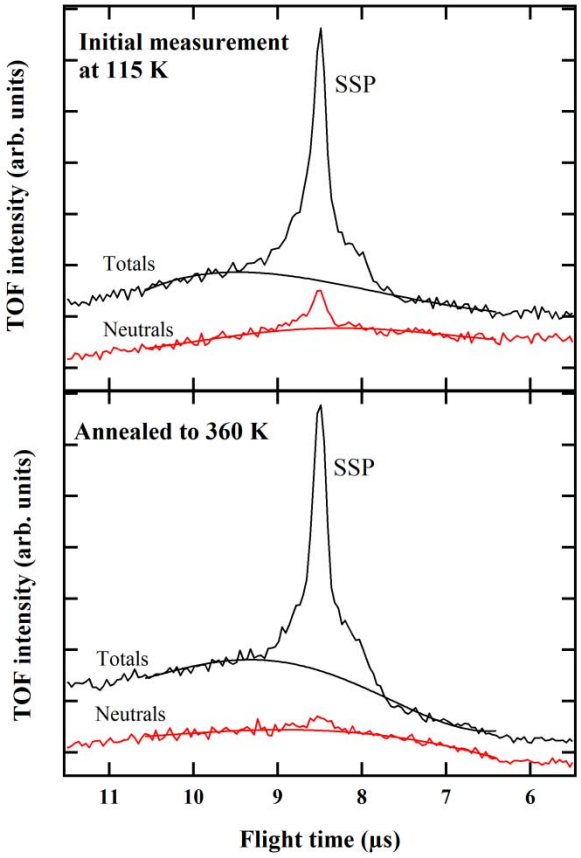

Figure 3.1: Time-of-flight spectra for 2.5 keV K+ scattered from 0.5 Å of Au deposited onto SiO_2 at 115 K (upper panel), and after annealing to 360 K (bottom panel). The upper curves in each graph are the total yields, while the lower curves show the scattered neutrals.

The SSP's from the total and neutral spectra of scattered K^+ are integrated to obtain the neutralization probability corresponding to a given surface temperature. The background resulting from recoiling light atoms (and other contributions) must first be subtracted before integration. The smooth lines in Fig. 3.1 show typical backgrounds

used, which were determined through a least-squares fit of a 4th order polynomial to the regions on both sides of the SSP. Even though the use of a polynomial to represent the background does not accurately account for the underlying physics of the scattering and recoiling processes, a visual inspection confirms that it does provide a reasonable approximation. Dividing the integrated neutrals signal by the integrated total yield signal provides the neutralization probability, or neutral fraction.

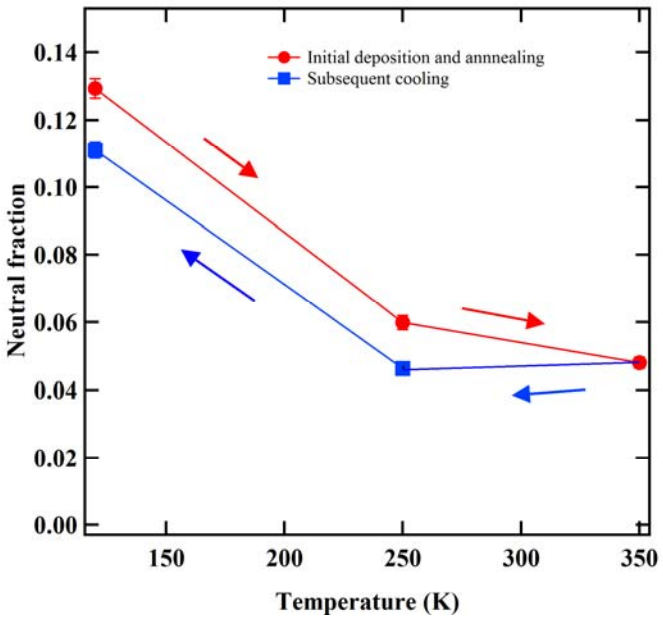

Figure 3.2 Neutral fraction for 2.5 keV K+ scattered from 0.5 Å of Au deposited onto SiO_2 as a function of sample temperature. The direction of the arrows shows the order in which the experiments were carried out. Error bars are shown for each point, but are not visible when smaller than the markers

Figure 3.2 shows the neutral fractions for 2.5 keV K^+ scattering from $Au/SiO_2/Si(111)$ as a function of the post-deposition surface temperature. The error bars indicate the statistical accuracy of the measurement, but do not include experimental variability, such as homogeneity of the material. The arrows show the order in which the measurements were carried out. The neutral fraction starts at 0.13 with a surface

temperature of 115 K, and then decreases to 0.05 as the surface temperature is raised to 360 K. When the surface is cooled to its original temperature, the neutral fraction increases back up to around 0.11.

3.4 Discussion

The neutralization of K^+ scattered from Au nanoclusters can be described within the context of the Resonant Charge Transfer (RCT) model, which has been successful in quantifying the neutralization of alkali ions scattered from metal surfaces [23]. A diagram illustrating the RCT process is shown in Fig. 3.3 for clusters adsorbed atop an insulating substrate. The figure shows a schematic of energy vs. distance from the surface, z. At the left is the SiO_2 substrate, which has a band gap of ~9 eV. States associated with the Au nanoclusters are illustrated schematically just to the right of the SiO_2. The dashed vertical line indicates the position of the surface plane. The potassium 4s ionization level is illustrated to the right of the surface plane, both when the projectile is far from and near to the surface.

The RCT model considers two electronic processes that occur simultaneously when the projectile nears the surface, as illustrated in the figure. First, the ionization level shifts upward as it interacts with its image charge in the surface. Second, the ionization level broadens because of overlap with states in the surface. When the projectile is sufficiently close to the surface, electrons tunnel back and forth, as represented by the horizontal arrow. Because the scattering process is very fast, the projectile spends very little time (femtoseconds) near the surface so that equilibrium is never established between the ionization level and the states in the solid. Thus, the

charge exchange is a non-adiabatic process that behaves as if the charge state distribution were "frozen in" at some point along the outgoing trajectory, rather than being determined by the relative energy level positions at infinite distance. To simplify the analysis, a position along the outgoing trajectory, beyond which the electrons can no longer tunnel, is often considered as an effective "freezing distance." The overlap of surface states with the broadened and shifted ionization level at this freezing distance represents the measured neutral fraction. As the ionization level typically overlaps the Fermi energy of the solid, the outgoing projectile is partially ionized at the freezing distance, which results in a measured neutralization probability between zero and one. A consequence of the RCT process is that when the surface work function increases, the neutralization probability decreases, and vice versa [15].

When scattering from nanoclusters, as opposed to bulk materials, the electronic structure of the clusters must be specifically considered. Because of quantum confinement effects, small metal nanoclusters have localized, discrete electronic states [20], as indicated schematically in Fig. 3.3. Kelvin Probe Force Microscopy (KPFM) studies [24] and simulations [25] have shown that these small clusters are often negatively charged, so that the filled portion of these quantum states can lie above the position of the Fermi level of the neutral bulk metal. Thus, more charge transfers from the nanoclusters to the scattered ions than would from a bulk metal surface. The additional neutralization associated with metal nanoclusters has been demonstrated for Ag on TiO_2 [14], Au on TiO_2 [14,26] and Au on SiO_2 [19]. Scattering from smaller clusters also results in more neutralization than with larger clusters, as shown in refs.

[13,14], in which the size was controlled by changing the amount of deposited metal. These studies show that the neutral fraction, collected at a given temperature, is a good indicator of the average size of the clusters.

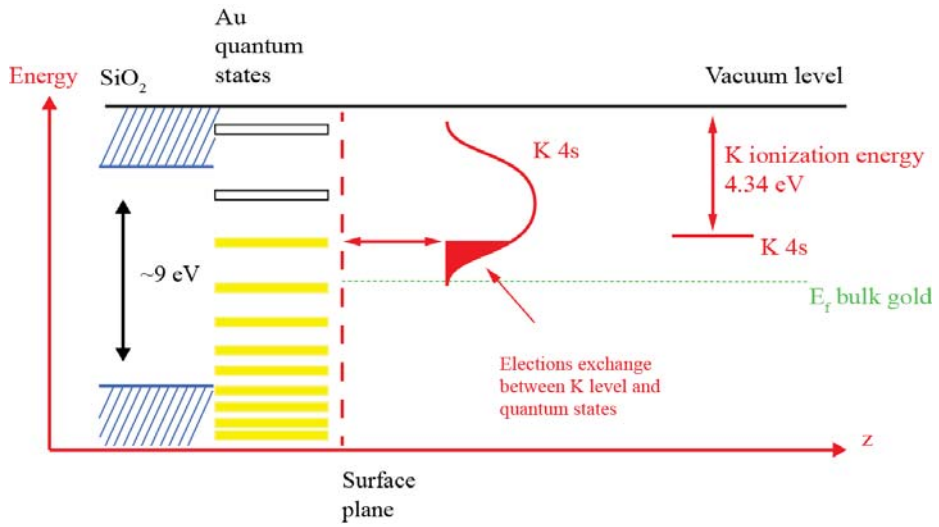

Figure 3.3 Schematic diagram illustrating the resonant charge transfer (RCT) process. The left side shows the band gap of the SiO_2 solid. The Au cluster states are shown for illustrative purposes and do not represent actual levels, with the solid boxes illustrating filled quantum states and the empty boxes representing empty states. The distance between the projectile and the surface is denoted as z. Note that the energy levels are not drawn to scale.

For the present data, however, it is unlikely that changes in the cluster size can explain the reversible dependence of the neutral fraction with surface temperature seen in Fig. 3.2. If the change in neutral fraction were representative of the cluster size, as in previous experiments, it would indicate that the clusters were agglomerating as the temperature rose, but then breaking apart again as the temperature fell. Such a reversible change in the cluster size distribution is not physically reasonable. Nor is it likely that the change in neutralization is driven by adsorbates coming from the background in the chamber, which could be reversibly physisorbed at low temperature, as we have since

reproduced these results at lower background pressures. Instead, it is more likely that the electronic structure changes as the temperature varies without changing the physical structure.

Note that thermally driven sintering of Au nanoclusters on SiO_2 has been observed with STM [27], but at higher temperatures than used in this experiment. In ref. [27], Au was deposited on SiO_2 at room temperature and then annealed to 800 K, which induced agglomeration. The work presented in this paper is conducted between 115 K and 360 K, however, which a much lower temperature regime than the one explored in ref. [27], so that agglomeration would not be expected.

In addition, there is evidence in the literature to suggest that agglomeration does not occur in this temperature regime. For one, thermal desorption experiments, which are also frequently carried out by cooling with liquid nitrogen and heating to room temperature, have been used to measure the chemical activity at nanocluster surfaces [8,28]. These experiments would have been irreproducible if the structure were significantly modified by the temperature ramp. Also, experiments done by Asscher and Goodman [8], in which the BLAG technique was applied repeatedly to a surface, yield a high density of small clusters. During each BLAG cycle, the temperature was ramped from 50 to 300 K. SEM images reveal that the average cluster size after one BLAG cycle is about the same as the average cluster size after seven BLAG cycles. This means that the clusters deposited during each individual cycle do not agglomerate as the temperature is ramped.

Thus, it is unlikely that significant changes in the cluster size distribution are occurring in the 120 - 360 K temperature range. Although some small amount of agglomeration could be responsible for the neutral fraction not quite returning to the original, as deposited, value, it can be concluded that the change in neutral fraction is driven primarily by a reversible electronic effect that is dependent on the temperature.

The temperature dependence is, however, in the opposite direction from what is expected. As the temperature increases, electronic states at higher energies should become occupied while states at lower energies become depopulated, in accordance with the Fermi-Dirac distribution. If the RCT model were correctly describing the neutralization process, it would be expected that the occupation of the higher energy electronic states should cause the neutral fraction to rise with temperature. Indeed, it was found that the neutralization of hyperthermal Na^+ scattered from clean Cu(001) was enhanced by increasing the surface temperature, in some cases by as much as a factor of three [16]. Surprisingly, an inverse correlation with temperature is found here.

Although this result does not make sense within the normal expectations for ion neutralization via RCT, it may be related to the unique electronic structure of supported nanoclusters. Unlike a bulk solid, nanoclusters have discrete electronic states that are localized at specific sites. Thus, the occupancy of the states that are accessible to the projectile during scattering may not be affected in the same way as bulk metal bands. For example, higher lying states may be populated when the temperature is raised, but these states may be localized more towards the interior of the clusters thereby reducing the occupancy of states at the surface of the clusters. Another possibility could be the

existence of electronic states associated with the metal/oxide interface, rather than with the clusters themselves. If such states were positioned at slightly higher energies than the cluster states so that they become occupied with increasing temperature, then states near the surface may be depleted when the temperature is raised. If either of these cases, electrons would no longer be visible to the scattering K^+ projectiles so that fewer of them would be neutralized.

Further experiments are planned to illuminate the underlying cause of this behavior, and test whether the ideas listed above could be correct. First, different alkali ions will be employed to reveal the effect that the ionization energy has on the temperature dependence. We have already observed a similar temperature dependence in preliminary measurements of 2 keV Na^+ scattering from Au/SiO_2, and will next use Li^+. Note that the neutralization of Li^+ has been previously shown to have an anomalous behavior when scattered from clusters [11], and this may be related to the same underlying physics as the inverse temperature dependence. The next planned experiments would employ a range of differing Au coverages to test whether the temperature dependence is a function of the cluster size. Finally, the incident energy will be varied to further probe the neutralization process, as the freezing distance changes with incident energy.

These planned measurements will provide insight into whether the above hypothesis is correct, i.e., whether thermal excitations are moving electrons away from cluster surface states and into buried cluster or interface states. The first ionization levels of Li, Na, and K are 5.39, 5.14 and 4.34 eV, respectively. If the effect is reproducible

with Na^+, it is likely that it will also be visible with Li^+ considering how close their ionization energies are. Furthermore, at higher impact energies, the ionization level broadening becomes more important than the relative positions of the electronic energy levels. Thus, if the negative temperature dependence were depressed for Li^+ and Na^+ because of their larger ionization energies relative to K^+, then the temperature dependence should be enhanced at higher incident energies as the smaller freezing distance would increase the overlap of the clusters states with the broadened ionization level. In addition, since larger clusters behave more like bulk Au, the negative temperature dependence should be less dramatic at higher Au coverages. Eventually, the negative temperature dependence should vanish or even reverse itself as a bulk-like film is formed.

3.5 Conclusions

While it had been previously established that the neutralization of alkali ions scattered from nanoclusters depends upon the size of the clusters, the incident energy of the ions and the identity of the projectile and target, the dependence on surface temperature had never been explicitly investigated. RCT theory and thermodynamics suggest that, if all else is identical, a higher surface temperature should lead to more neutralization. These experiments reveal, however, that the neutral fraction for K^+ scattering from Au nanoclusters reversibly decreases with increasing sample temperature. Agglomeration of the nanoclusters with temperature and physisorption of contaminants were ruled out as primary explanations for this behavior. We conclude there is an explicit and reversible electronic effect that drives down the neutral fraction with increasing

temperature. This effect may be related to the localized nature of the thermal excitations. It is clear that more experiments are needed to fully explain why the temperature dependence of the neutralization probability is opposite from expectations.

Chapter 3 bibliography

1. L. Armelao, D. Barreca, G. Bottaro, A. Gasparotto, S. Gross, C. Maragno, and E. Tondello, Coord. Chem. Rev. **250**, 1294 (2006).

2. F. Buatier de Mongeot and U. Valbusa, J. Phys.: Condens. Matter **21**, 224022 (2009).

3. G. S. Aluri, A. Motayed, A. V. Davydov, V. P. Oleshko, K. A. Bertness, N. A. Sanford, and R. V. Mulpuri, Nanotechnology **23**, 175501 (2012).

4. M. S. Chen and D. W. Goodman, Science **306**, 252 (2004).

5. J. P. Wilcoxon and B. L. Abrams, Chem. Soc. Rev. **35**, 1162 (2006).

6. P. Karmakar, G. F. Liu, Z. Sroubek, and J. A. Yarmoff, Phys. Rev. Lett. **98**, 215502 (2007).

7. J. S. Palmer, P. Swaminathan, S. Babar, and J. H. Weaver, Phys. Rev. B **77**, 195422 (2008).

8. E. Gross, M. Asscher, M. Lundwall, and D. W. Goodman, J. Phys. Chem. C **111**, 16197 (2007).

9. A. Keller and S. Facsko, Materials **3**, 4811 (2010).

10. E. Chason and W. Chan, Top. Appl. Phys. **116**, 53 (2010).

11. G. F. Liu, Z. Sroubek, P. Karmakar, and J. A. Yarmoff, J. Chem. Phys. **125**, 054715 (2006).

12. M. Valden, X. Lai, and D. W. Goodman, Science **281**, 1647 (1998).

13. G. F. Liu, Z. Sroubek, and J. A. Yarmoff, Phys. Rev. Lett. **92**, 216801 (2004).

14. A. R. Canario and V. A. Esaulov, J. Chem. Phys. **124**, 224710 (2006).

15. J. Los and J. J. C. Geerlings, Phys. Rep. **190**, 133 (1990).

16. C. E. Sosolik, J. R. Hampton, A. C. Lavery, B. H. Cooper, and J. B. Marston, Phys. Rev. Lett. **90**, 013201 (2003).

17. Y. Yang and J. A. Yarmoff, Surf. Sci. **573**, 335 (2004).

18. R. Singh, Microelectron. J. **23**, 273 (1992).

19. S. Balaz and J. A. Yarmoff, Surf. Sci. **605**, 675 (2010).

20. S. Balaz and J. A. Yarmoff, J. Phys.: Condens. Matter **22**, 084009 (2010).

21. B. Peko and T. Stephen, Nucl. Instrum. Meth. B **171**, 597 (2000).

22. H. Niehus, W. Heiland, and E. Taglauer, Surf. Sci. Rep. **17**, 213 (1993).

23. G. A. Kimmel and B. H. Cooper, Phys. Rev. B **48**, 12164 (1993).

24. H. J. Chung, A. Yurtsever, Y. Sugimoto, M. Abe, and S. Morita, Appl. Phys. Lett. **99**, 123102 (2011).

25. A. Sanchez, S. Abbet, U. Heiz, W.-D. Schneider, H. Häkkinen, R. N. Barnett, and U. Landman, J. Phys. Chem. A **103**, 9573 (1999).

26. G. F. Liu, P. Karmakar, and J. A. Yarmoff, J. Vac. Sci. Technol. A **25**, 1133 (2007).

27. W. T. Wallace, B. K. Min, and D. W. Goodman, Top. Catal. **34**, 17 (2005).

28. W. E. Kaden, W. A. Kunkel, F. S. Roberts, M. Kane, and S. L. Anderson, J. Chem. Phys. **136**, 204705 (2012).

Chapter 4

Low energy ion scattering investigation of thermally induced agglomeration of Au nanoclusters on SiO_2

4.1. Introduction

Metal nanoclusters supported on oxide surfaces have potential for use in diverse applications, such as catalysis [1] and sensors [2]. Many methods have been used to deposit metal nanoclusters onto substrates including physical vapor deposition (PVD), chemical vapor deposition, sol-gel solutions, and RF sputtering [3]. After deposition, the distribution of cluster sizes and shapes can be altered by a thermal treatment. Since the unique properties of nanoclusters are related to their novel electronic states, the evolution of these states with the structural changes that occur upon annealing has implications for the robustness of devices and processes. Moreover, an appropriate thermal process could be used to purposefully tune the properties of devices. While there have been studies of the effects of annealing on cluster size and morphology [4-6], these have mostly used scanning tunneling microscopy (STM) to measure clusters adsorbed onto flat, well-ordered materials. Here, we report a new methodology for the use of low energy ion scattering (LEIS) to measure the evolution of cluster sizes that can be applied to a more diverse set of materials.

LEIS has traditionally provided information on the atomic structure and composition of solid surfaces through measurements of the energy and angular distributions of the scattered ions [7,8]. The surface local electrostatic potential (LEP) can also be ascertained through the neutralization probability of the scattered ions when

employing projectiles with low ionization potentials, such as alkalis. LEIS has been used to detect variations in the LEP by monitoring the neutralization for scattering from different surface sites [9-12] and by the trajectory dependence of the neutralization [13-17]. In addition, the neutralization of scattered alkali ions is sensitive to filled electronic states in nanoclusters, the occupancy of which is related to their shape and size [18-20].

Previous studies have shown that the shapes and sizes of metal clusters on oxide surfaces can be controlled through either the coverage or the substrate temperature. When a metal is deposited by PVD onto an oxide, it often forms small clusters due to mismatch in the respective surface energies. For clusters deposited at room temperature, the average size increases with metal coverage [21]. The PVD deposited clusters form with a distribution of sizes that coarsens with annealing [4,6]. There are two models regularly employed to describe how clusters change size with annealing. The first is Ostwald ripening, in which atoms preferentially detach from the clusters and diffuse along the surface to become attached to larger clusters, resulting in the growth of large clusters along with formation of smaller ones and a lowering of the total energy of the system [22]. The second is coalescence, also called sintering or agglomeration, during which intact clusters move about the surface until they find another cluster and stick together leading to an increase in the size of clusters. In addition, previous STM studies have shown a more complicated behavior for Pd/TiO_2, called "static coalescence," in which clusters agglomerate locally without changing their center of mass [23]. Similar processes have also been observed for Au/SiO_2 with STM, albeit at lower temperatures [24].

Although microscopy techniques such as STM, scanning electron microscopy (SEM), and transmission electron microscopy (TEM) are good tools to study the evolution of cluster sizes and shapes, LEIS has some advantages over these techniques. Because LEIS is not sensitive to local temperature variations, it can be carried out rapidly over a broad range of temperatures. In contrast, STM will not produce useful images until the temperature of the instrument stabilizes. Since ion scattering does not require that the surfaces be particularly smooth, information can be obtained from nanoclusters resident on a disordered substrate, such as a heavily sputtered oxide, which is not possible with STM. In addition, LEIS probes the average distribution over a macroscopic region of the surface, typically about 1 mm^2, rather than focusing on a microscopic area and assuming that the material is uniform. Furthermore, the clusters of interest are often only a few nanometers in diameter, a resolution that is not easily achieved with SEM. TEM, which can obtain atomic resolution, requires that the substrate be amorphous, while most common substrates are crystalline, including Si(111), which is used in the present work. Also, SEM and TEM are generally *ex-situ* techniques that require the transport of the samples through air, which can modify the nanoclusters.

This chapter introduces a new method for analyzing charge-resolved time-of-flight (TOF) alkali LEIS spectra to reveal information about the size distribution of supported metal nanoclusters. Both the neutralization and the relative proportions of single scattering (SS) and multiple scattering (MS) depend on the cluster size, but in different ways. An analysis that involves comparison of these two observables is used to monitor the evolution of the cluster size distribution with annealing. It is shown that, on

average, the multiply scattered ions are neutralized more efficiently as the surface is annealed to higher temperatures. This leads to the conclusion that some of the annealed nanoclusters agglomerate, while most of the smaller clusters change their shape.

4.2. Experimental procedure

The measurements were carried out in an ultra-high vacuum (UHV) chamber with a base pressure below $2x10^{-10}$ torr. Si(111) wafers (n-type, 5-10 Ω cm) were mounted on a commercial button heater (Heatwave Labs) attached to an x-y-z sample manipulator. The surface was sputtered *in situ* with 500 eV Ar^+ to remove the native oxide and any contaminants, such as adsorbed hydrocarbons. The sample was next annealed to 1173 K for one minute to restore the crystallinity. A thin, uniform thermal oxide film was produced by heating the clean Si to 973 K in $1x10^{-5}$ torr of dry oxygen (O_2) [25]. During oxidation, the O_2 flowed continuously from the leak valve into a turbomolecular pump to maintain purity. The surface was allowed to cool to 550 K before evacuating the O_2 to prevent pinholes from forming in the oxide layer [26]. Auger electron spectroscopy was used to monitor the oxide surface. After oxidation, the surface was found to contain about 8% carbon. While this is more contamination than would be ideal, it does not affect the properties investigated here.

Gold (Au) was deposited onto the surface from a homemade evaporator, consisting of a tungsten filament (Mathis) wrapped with 99.98% Au wire (ESPI). The evaporation rate was 0.021 Å sec^{-1} as calibrated with a quartz crystal microbalance. Au

coverages of 0.5, 1.0 and 2.0 Å, which correspond to increasing initial cluster sizes [27], were employed for these experiments.

Time-of-flight (TOF) LEIS spectra were collected for 2 keV Na^+ ions at a scattering angle of 135° and normal emission, as described previously [28]. The ions were produced from a thermionic emitter gun (Kimball Physics). The beam was rastered across a 1 mm diameter aperture to produce pulses at 40 kHz with a pulse width of about 100 ns. The TOF detector is a dual microchannel plate (MCP) array mounted at the end of a 0.67 m long drift tube. The front of the MCP detector is held at ground so that scattered ions and neutrals arrive with the same kinetic energy and thus have the same detection efficiency [29]. A time-to-digital converter (Stanford) measures the time differences between the ion gun pulses and the scattered particles arriving at the detector. These time differences are histogrammed to create a TOF spectrum. The TOF flight tube contains a pair of electrostatic deflection plates used to remove the scattered ions and collect a neutrals-only spectrum. The collection of total yield and neutrals spectra is alternated every minute, using a computer-controlled 300 V power supply, which minimizes effects of long-term drift in the incident beam current.

Spectra were collected at room temperature from the as-deposited material, and after the samples had been annealed to a series of increasing temperatures for 5 minutes each up to 1000 K. After each anneal, the sample was allowed to cool to at least 350 K before a TOF spectrum was collected. This disentangles the effects of morphological changes from the temperature dependence of the neutralization process itself.

Note that an explicit temperature dependence was observed for the neutralization of K^+ scattered from Au on SiO_2 [30], which suggests that it could be important to collect all spectra at a constant temperature. K is heavier than the Na used in the present measurements, however, so that it travels more slowly and is thus more sensitive to thermal excitations of electrons near the Fermi energy. To determine how important it is to maintain a fixed temperature for Na^+ scattering, the neutralization in scattering from Au nanoclusters was compared at 100 and 300 K and found to be unchanged. Thus, maintaining a precise temperature is not critical for charge exchange experiments that employ 2 keV Na^+ ions.

4.3. Results

Figure 4.1 shows raw TOF spectra of 2 keV Na^+ scattered from 2 Å of Au deposited onto SiO_2. The upper trace represents the total yield of the scattered particles, while the lower trace indicates the projectiles that had neutralized during scattering. The spectra are each dominated by a single scattering peak (SSP), which corresponds to Na^+ ions that have backscattered directly from Au atoms on the surface. Because Na is heavier than O and almost as heavy as Si, it cannot backscatter from any of the substrate atoms via a single collision at the large angle employed for these measurements. Thus, the SSPs arise solely from the deposited Au.

Single scattering is not the only way that an ion scattered from Au can reach the detector, however. At higher energies than the SSP is the plural scattering (PS) region, which represents ions that have undergone two or more in-plane collisions with Au atoms. For example, in the instance of quasi-double (QD) scattering, the projectile

experiences two hard collisions through larger angles within the scattering plane that result in a total scattering angle of 135° and, in doing so, loses less energy than scattering once through 135° [7,31,32]. At lower energies than the SSP is the multiple scattering region [31]. A multiply scattered ion penetrates the surface and interacts with several atoms in the interior of a Au cluster, not necessarily in the same plane, before being emitted and reaching the detector. Projectiles scattering in this manner usually lose more energy than singly scattered particles.

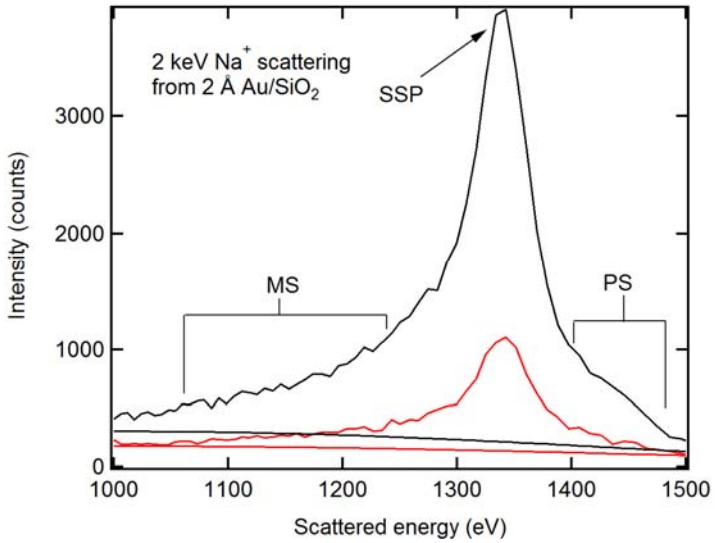

Figure 4.1. Raw TOF spectra of 2 keV Na^+ scattering from 2 Å Au on SiO_2. The total (upper curve) and neutral (lower curve) yields are both shown, as are the calculated backgrounds

In addition to scattering processes, the detector can also register an event due to recoiled Si or O atoms. Because the Na scattered from Au rides on top of a background of recoiled atoms, it is necessary to subtract an appropriate background before doing any

quantitative analysis [30]. These backgrounds are approximated by fitting 4th order polynomials to the spectra after excluding the region that contains scattering from Au.

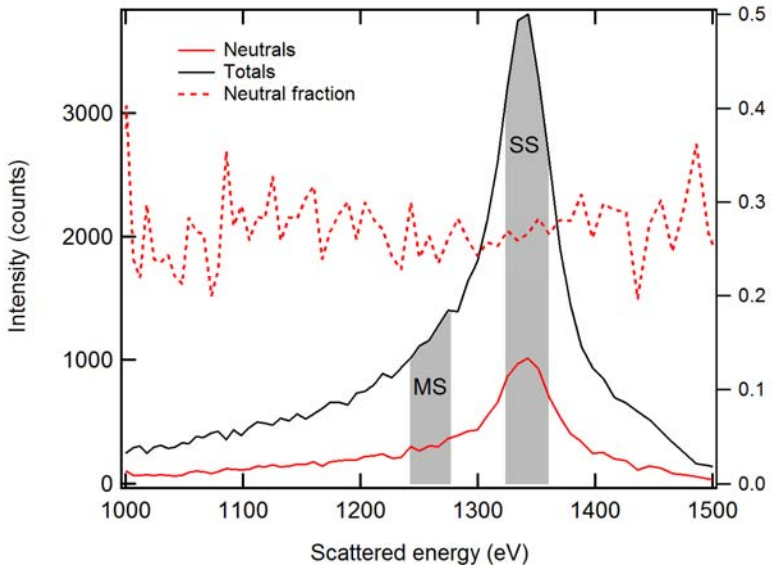

Figure 4.2. Totals and neutrals TOF spectra for 2 keV Na^+ scattering from 2 Å Au on SiO_2 after subtracting the backgrounds. The region used for calculating neutral fractions is highlighted.

Figure 4.2 shows the same TOF spectra as Fig. 4.1 after background subtraction. The resulting spectra are flat and close to zero away from the Au scattering peaks, suggesting that the calculated background is a reasonable approximation, even if it does not use a physically correct model for the recoiled Si and O atoms.

This figure also shows the neutral fraction calculated point-by-point by dividing the neutral by the total yield. To determine the neutralization associated with specific trajectory types, regions are designated as "single scattering" and "multiple scattering". These regions, which are highlighted in grey, are used to calculate the quantities presented in Figs.4.3 and 4.4. For single scattering, neutral fractions were calculated by

averaging five points centered about the highest point in the SS region. The MS region is selected to be far enough away from the SSP that it contains almost exclusively multiple scattering, while it is made large enough to give statistically meaningful results. The MS neutral fractions are calculated by averaging the point-by-point data over the designated region. The error bars for SS and MS neutral fractions are determined from the scatter in the point-by-point neutral fractions within the region.

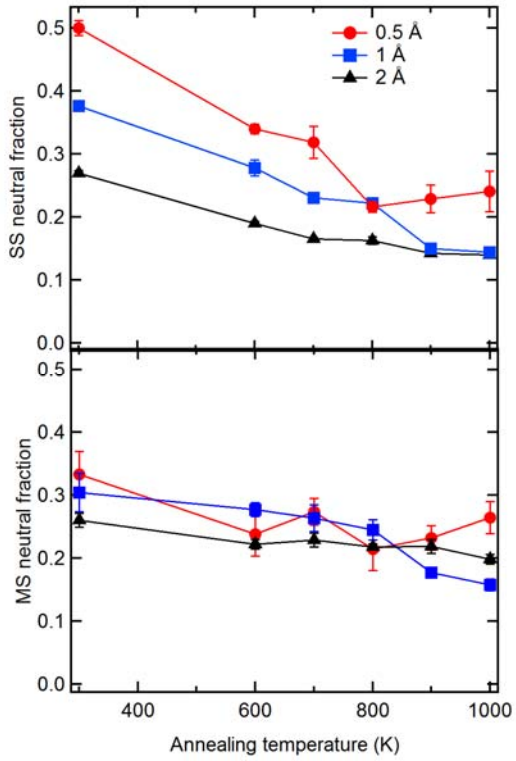

Figure 4.3. Single and multiple scattering neutral fractions as a function of annealing temperature for each of the three coverages employed.

Figure 4.3 shows the SS and MS neutral fractions as a function of annealing temperature for the three coverages investigated. Before annealing, the single scattering neutral fractions shown in the upper panel are larger for the smaller coverages of Au, starting at 0.50 for the smallest coverage of 0.5 Å, 0.38 for the 1 Å coverage, and 0.27 for

the 2 Å coverage. After annealing, the single scattering neutral fractions for the 1 Å and 2 Å coverages converge at about 0.14, while the data for the 0.5 Å coverage decreases to 0.22 and then levels off. There is a general increase in uncertainty as the annealing temperature increases, but this is not true for every point. The multiple scattering neutral fractions, shown in the lower panel, are less dependent on the annealing temperature as they slightly decrease with temperature and range between 0.2 and 0.3. Although the multiple scattering neutral fraction data is not very illuminating by itself, the ratio of multiple scattering to single scattering neutral fractions is very useful.

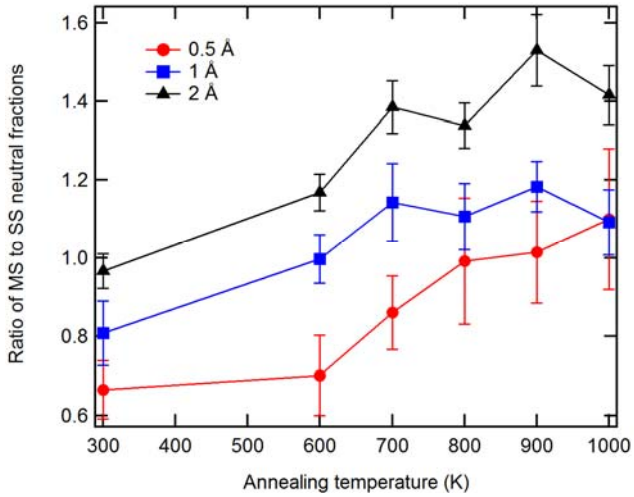

Figure 4. Ratio of the neutral fractions of multiply scattered ions to those of singly scattered ions.

Figure 4.4 shows the ratio of the neutral fraction of the MS region to the neutral fraction of the SS region, which we will refer to as "R," as a function of annealing temperature for the three metal coverages. Analysis will show that this parameter provides a dimensionless characterization of cluster sizes and shapes. A value of 1 means that, on average, the neutral fractions of the singly and multiply scattered ions are the same. A value greater than 1 means that the multiply scattered ions are overall more

efficiently neutralized, while a value less than 1 means that the singly scattered ions are more efficiently neutralized. In almost all cases, this ratio increases with annealing temperature and coverage.

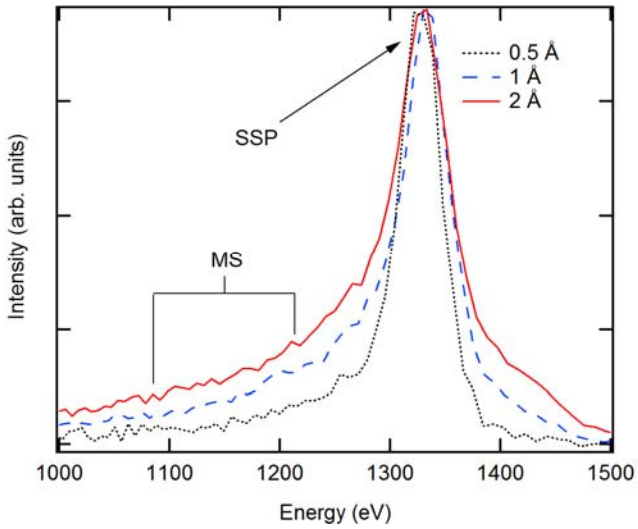

Figure 4.5. Total scattered yield of 2 keV Na^+ ion scattering from as-deposited clusters for 0.5 Å, 1 Å, and 2 Å of Au. The 0.5 Å and 1 Å spectra have been scaled so that the SSPs match.

Figure 4.5 shows TOF spectra for 2 keV Na^+ ions scattering from 0.5 Å, 1 Å, and 2 Å of Au as deposited on SiO_2. The 0.5 Å and 1 Å data have been scaled to match the height of the 2 Å SSP and illustrate how the proportion of MS changes with increasing deposition. While it is well known that cluster size increases with deposition, it is not clear that larger clusters would necessarily give rise to more multiple scattering, since clusters above a certain size would appear bulk-like from a scattering kinematics perspective. The spectra in Fig. 4.5, however, show a clear increase in the proportion of

multiple scattering with Au deposition, demonstrating that the data is sensitive to cluster size in the range typical of this experiment.

4.4. Discussion

Neutralization of alkali ions during LEIS is usually described in terms of the Resonant Charge Transfer (RCT) model [33]. RCT considers two electronic processes that occur as the ion approaches the surface. First, the Na 3s level shifts upward in energy as it interacts with its image charge. Second, the ionization level broadens because of overlap with states in the material. In the adiabatic limit, the electrons would find the lowest energy state when scattering, resulting in a neutralization probability of either zero or one depending on whether the ionization energy lies above or below the surface Fermi level. Because the ion spends a small amount of time near the surface (on the order of femtoseconds) as compared to the amount of time it takes to neutralize, however, the process during LEIS is non-adiabatic, which produces an intermediate value of the neutral fraction. This measured neutral fraction is acutely sensitive to the local electrostatic potential (LEP) just above the scattering site [9], which is sometimes referred to as the local work function. The specific point above the surface at which the potential is probed is labeled the "freezing distance".

In the case of nanoclusters, it is necessary to consider the clusters' specific electronic structure. It has been shown that metal nanoclusters resident on an oxide surface neutralize alkali ions more efficiently than a bulk metal [34], even more so than the potential associated with the work function measured by a secondary electron cutoff spectrum would suggest [18]. To explain this, it was proposed that the nanoclusters have

quantum-confined states that act to modify the surface LEP and drive the neutralization. The result is that the neutralization is dependent on the size of the clusters, with smallest clusters giving rise to the largest neutral fractions.

In addition to the size dependence of the neutralization, the proportion of multiple to single scattering also depends on the sizes and shapes of the clusters, as indicated by the data in Fig. 4.5. The single scattering yield is basically proportional to the number of atoms that are directly visible to the beam and the TOF detector, while the multiple scattering yield is roughly proportional to the number of surface atoms with many neighbors. Thus, in general, larger clusters will produce relatively more multiple scattering than smaller ones. The shapes are also important, however, as a cluster consisting of only a few atomic layers will produce very little multiple scattering, while the multiple scattering yield will increase for the same number of atoms if they are arranged into a 3D shape.

Because the probability for MS has a different dependence on cluster size and shape than the neutralization probability, it is possible that the measured single and multiple scattering yields, which are averages over the entire surface, will have different neutralization probabilities when the cluster size distribution is inhomogeneous. The data in Fig. 4.4 shows that the neutral fractions for single and multiple scattering are not always the same, i.e., R is not equal to 1, even immediately after deposition. Furthermore, the ratio R changes with annealing, which indicates that the size and shape distribution has been modified.

An R value less than 1 occurs when the multiple scattering is dominated by sites that are less efficient at neutralizing the scattered projectiles. For example, the cluster distribution could be composed of a mixture of very small and flat clusters along with larger and taller clusters. Because the flat clusters will contribute little to multiple scattering, the MS neutral fraction will be determined primarily by the large clusters. The SS neutral fraction, on the other hand, will be a weighted average of the small cluster and large cluster neutral fractions. Thus, in total, the singly scattered particles will be more efficiently neutralized and R will be less than 1.

In contrast, a value of R greater than 1 occurs when the multiple scattering is dominated by scattering sites that have a high efficiency for neutralization. In this case, the surface could contain a mixture of small clusters that are three-dimensional in shape along with larger clusters. Highly three-dimensional structures can produce more multiple scattering than the same atoms arranged as a flat cluster, so the multiple scattering neutral fraction will be enhanced compared to the single scattering neutral fraction and R could exceed 1.

Analysis of R as a function of metal deposition and annealing temperature can be used to determine the effects of annealing. The value of R increases with annealing, suggesting that the clusters that are efficient at neutralization become more three-dimensional during the annealing process, while some of larger clusters may agglomerate.

To illustrate how an increase in R is consistent with this conclusion, we constructed a simplified model in which some reasonable guesses are made about the

relative proportions of single and multiple scattering as a function of cluster size and shape. In this model, four types of clusters are employed to construct a collection of clusters believed to be representative of the types of clusters that may be present on the surface. It is assumed that these are the only clusters present, but that annealing enables clusters to convert from one type to another. These four cluster types are listed in Table

	Cluster type	SS yield	MS yield	Neutral fraction
A	Small and flat	3	0	0.5
B	Medium and 3D	4	5	0.25
C	Small and 3D	1	3	0.5
D	Large	5	8	0.1

Table 4.1. Types of clusters that are used to model the evolution of the surface with annealing.

4.1 along with their assigned characteristics. The first two clusters, denoted "A" and "B", are assumed to be present on the as-deposited surface. "A" clusters are so flat that they do not produce any multiple scattering and small enough to have a high neutralization probability. "B" clusters are medium sized and somewhat three dimensional, exhibiting some multiple scattering and some single scattering with an intermediate neutralization probability. The final two clusters, denoted "C" and "D," are assumed to the majority type of clusters present on the annealed surface. "C" type clusters are small and three-dimensional, exhibiting more multiple scattering along with a high neutralization probability. "D" type clusters are large, exhibiting a large amount of scattering in general while having a low neutralization probability.

The cluster size distributions used in the model are detailed in Table 4.2 for pre- and post-annealing. Agglomeration of clusters is simulated by reducing the number of

small clusters in the post-annealed system while increasing the amount of scattering in the larger clusters. The neutral fraction is modeled as being strongly dependent only on the number of atoms in the cluster, and not the cluster shape, so that the clusters that do not agglomerate retain the same neutral fraction, while the neutral fraction of the agglomerated clusters decreases. This is a clearly an oversimplification as the neutral fraction may also depend on the cluster shape, but we can still demonstrate how the ratio R depends on changing cluster shapes without including that complication in the model. For the purposes of this analysis, it is also assumed that the LEP is uniform across a given cluster, so that the ion's neutralization probability is determined by the potential above the cluster it scatters from, and not the details of the ion's trajectory as it scatters from that cluster. Thus, the neutralization from a given cluster will be the same whether a projectile undergoes SS or MS.

With this description of the model in place, it can now be employed using an arbitrary system of units to predict some of the qualitative features of the experimental data. Using the parameters outlined in Table 4.1, we show how R is sensitive to the distribution of cluster sizes and shapes. The R value for a given cluster size distribution is calculated by determining the neutralization probability for both singly scattered and multiply scattered particles, then dividing the MS neutral fraction by the SS neutral fraction.

To illustrate the model, the calculation of the SS neutral fraction for the as-deposited surface will now be outlined. As shown in Table 4.2, the model for the as-deposited surface contains 8 clusters of type A and 2 clusters of type B. The type A

clusters support 24 units of single scattering in all, and the type B clusters support 8 units of single scattering, for a total of 32 units of single scattering. Of the 24 units of single scattering from the type A clusters, 12 units will be neutralized, as per their associated

System	# A	# B	# C	# D	SS neutral fraction	MS neutral fraction	R
As deposited	8	2	0	0	0.44	0.25	0.57
Annealed	0	0	6	2	0.25	0.29	1.16

Table 4.2. Number of each type of clusters in the as-deposited and annealed surfaces as used in the model, neutral fractions, and R-values for each.

neutral fraction listed in Table 4.1. Similarly, of the 8 units of single scattering from the type B clusters, 2 will be neutralized. Thus, 14 units of the single scattering will be neutralized out of the 32 units in all, which yields a neutral fraction of 0.43. The other neutral fractions are calculated in a similar way, and the R values for each surface are calculated by appropriate division.

The results of the model match some of the broad features of the data collected. First, it shows that R can be either less than 1 or greater than 1 depending on the details of the clusters' structure and their distribution on the surface. An R value less than 1 signifies an inhomogeneous distribution of clusters that are mostly flat and support little multiple scattering, so that a proportionally greater number of the singly scattered ions are neutralized. Alternatively, an R value greater than 1 signifies that more multiply scattered ions are coming from the high efficiency neutralization sites. Thus, an increasing value of R signifies a transition from a system dominated by two-dimensional structures to a system dominated by three-dimensional structures.

The model also makes some other useful predictions. For instance, it predicts that agglomeration alone is not sufficient to explain the enhanced multiple scattering. If some clusters agglomerated as in the model, but the smaller clusters did not change their shape, the single scattering would exhibit more efficient neutralization than the multiple scattering. In that case, the high neutralization clusters would not participate in multiple scattering, and so the multiple scattering neutral fraction would not be enhanced. In addition to explaining the enhancement of the multiple scattering, the model also predicts a dramatic decrease in single scattering and a modest increase in multiple scattering. Figure 4.6 shows the total scattered yield from 0.5 Å of Au on SiO_2, both as deposited and after annealing to 600 K. As predicted by the model, there is about a factor of 2 decrease in the single scattering yield and a modest increase in the multiple scattering yield.

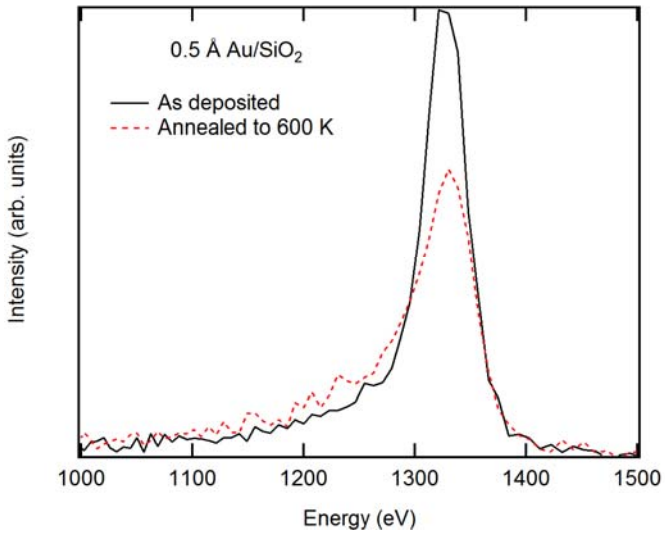

Figure 4.6. Comparison of TOF spectra of 0.5 Å Au on SiO_2, as deposited and after annealing to 600 K. The spectra are normalized to equal Na^+ ion fluence.

Previous STM studies of Au/SiO_2 have confirmed that the clusters become less homogeneous after annealing [24]. Annealing to 200°C for 3 hours creates a mixture of large and small clusters on the surface. Furthermore, the majority of the clusters do not change their size, while at the same time the average cluster size increases, suggesting that the smaller clusters become more three-dimensional as they ripen.

While the value of R reveals information about the distribution of the shapes of the clusters, the single scattering neutral fraction reveals information about the clusters' average size. Our data almost exclusively shows a decrease in neutral fraction with annealing. This would indicate that the average cluster size is increasing with annealing temperature. For a surface with both large and small clusters, larger clusters will be overrepresented in the ion scattering signal because they cover more area. Evidently, the surface area is dominated by larger clusters with increasing annealing temperature. For depositions greater than 0.5 Å, annealing to 900 K creates a surface dominated by electronically bulk-like gold.

As the cluster sizes increase, there is a lower limit to the neutral fraction as bulk-like gold is formed. The data shows a minimum neutral fraction of 0.14 for both the 1 Å and 2 Å data sets, suggesting that electronically bulk-like gold is formed. Under the scattering conditions described in this paper, polycrystalline gold has been found to have a neutral fraction of 0.10 [35]. The discrepancy in the neutral fractions between the polycrystalline surface and the gold annealed at a high temperature is small, and likely caused by the persistence of a small number of high neutralization scattering sites, such as a few particularly stable small clusters.

4.5. Conclusions

Surfaces with inhomogeneous cluster size distributions give rise to different neutralizations for SS and MS. Thus, analyzing the difference between the SS and MS neutral fractions can yield information about the cluster size distribution. We found that multiply scattered ions are more efficiently neutralized than singly scattered ions for annealed Au/SiO_2. This effect increases with higher temperature and higher coverage. This enhanced neutralization is attributed to a simultaneous agglomeration of some, but not all, of the clusters, while the remaining cluster change their shape without changing their size.

Although this information could be gathered from STM for the system studied here, this technique is nevertheless developed for use on other systems not amenable to STM. Furthermore, the choice of Au/SiO_2 allows for follow-up studies where STM can be used to corroborate the conclusions made here. One such experiment would be to combine STM with simultaneous ion scattering spectroscopy to observe the distribution of cluster sizes as it develops, as well as the cluster distribution's effect on neutralization. Furthermore, it would help to determine whether Au/SiO_2 undergoes static coalescence during annealing, similar to Pd/TiO_2, or Ostwald ripening for the annealing conditions and coverages used here. Information gathered from STM could also be used to inform a simulation which would determine if the single and multiple scattering yield can be explained by the observed cluster size distributions.

Chapter 4 bibliography

1. G. Li, D. E. Jiang, C. Liu, C. L. Yu, and R. C. Jin, J. Catal. **306**, 177 (2013).
2. G. S. Aluri, A. Motayed, A. V. Davydov, V. P. Oleshko, K. A. Bertness, N. A. Sanford, and R. V. Mulpuri, Nanotechnology **23** (2012).
3. L. Armelao, D. Barreca, G. Bottaro, A. Gasparotto, S. Gross, C. Maragno, and E. Tondello, Coord. Chem. Rev. **250**, 1294 (2006).
4. W. T. Wallace, B. K. Min, and D. W. Goodman, Top. Catal. **34**, 17 (2005).
5. P. R. Gadkari, A. P. Warren, R. M. Todi, R. V. Petrova, and K. R. Coffey, J. Vac. Sci. Technol., A **23**, 1152 (2005).
6. L. Sungsik, F. Chaoyang, T. Wu, and S. L. Anderson, Surf. Sci. **578**, 5 (2005).
7. H. H. Brongersma, M. Draxler, M. de Ridder, and P. Bauer, Surf. Sci. Rep. **62**, 63 (2007).
8. C. J. Jenks and R. Bastasz, Prog. Surf. Sci. **75**, 147 (2004).
9. C. B. Weare and J. A. Yarmoff, Surf. Sci. **348**, 359 (1996).
10. C. B. Weare, K. A. H. German, and J. A. Yarmoff, Phys. Rev. B **52**, 2066 (1995).
11. K. A. H. German, C. B. Weare, P. R. Varekamp, and J. A. Yarmoff, J. Vac. Sci. Technol. A **11**, 2260 (1993).
12. R. Souda, E. Asari, H. Kawanowa, T. Suzuki, and S. Otani, Surf. Sci. **421**, 89 (1999).
13. G. F. Liu, P. Karmakar, and J. A. Yarmoff, Phys. Rev. Lett. **98**, 176104 (2007).
14. G. F. Liu and J. A. Yarmoff, Surf. Sci. **600**, 2293 (2006).
15. V. A. Morozov and F. W. Meyer, Phys. Rev. Lett. **86**, 736 (2001).

16. R. Beikler and E. Taglauer, Nuclear Instruments & Methods in Physics Research Section B-Beam Interactions with Materials and Atoms **182**, 180 (2001).

17. L. Q. Jiang, Y. D. Li, and B. E. Koel, Phys. Rev. Lett. **70**, 2649 (1993).

18. G. F. Liu, Z. Sroubek, P. Karmakar, and J. A. Yarmoff, J. Chem. Phys. **125**, 054715 (2006).

19. A. R. Canario and V. A. Esaulov, J. Chem. Phys. **124**, 224710 (2006).

20. P. Karmakar, G. F. Liu, Z. Sroubek, and J. A. Yarmoff, Phys. Rev. Lett. **98**, 215502 (2007).

21. X. Lai, T. P. S. Clair, M. Valden, and D. W. Goodman, Prog. Surf. Sci. **59**, 25 (1998).

22. P. A. Thiel, M. Shen, D. J. Liu, and J. W. Evans, J. Phys. Chem. C **113**, 5047 (2009).

23. R. A. Bennett, D. M. Tarr, and P. A. Mulheran, J. Phys.-Condes. Matter **15**, S3139 (2003).

24. A. Berlinger, Applied Physics a-Materials Science & Processing **68**, 403 (1999).

25. Y. Yang and J. Yarmoff, Surf. Sci. **573**, 335 (2004).

26. R. Tromp, G. W. Rubloff, P. Balk, F. K. Legoues, and E. J. Vanloenen, Phys. Rev. Lett. **55**, 2332 (1985).

27. M. Valden, X. Lai, and D. W. Goodman, Science **281**, 1647 (1998).

28. S. Balaz and J. A. Yarmoff, Surf. Sci. **605**, 675 (2010).

29. M. Barat, J. C. Brenot, J. A. Fayeton, and Y. J. Picard, Rev. Sci. Instrum. **75**, 2050 (2000).

30. A. B. Arjad and J. A. Yarmoff, Nucl. Instrum. Meth. B (2013).

31. H. Niehus, W. Heiland, and E. Taglauer, Surf. Sci. Rep. **17**, 213 (1993).

32. S. B. Luitjens, A. J. Algra, E. Suurmeijer, and A. L. Boers, Surf. Sci. **99**, 652 (1980).

33. J. Los and J. J. C. Geerlings, Phys. Rep. **190**, 133 (1990).

34. G. F. Liu, Z. Sroubek, and J. A. Yarmoff, Phys. Rev. Lett. **92**, 216801 (2004).

35. R. Sanderson and J. A. Yarmoff, unpublished.